






# Cobalamin Riboswitches Are Broadly Sensitive to Corrinoid Cofactors to Enable an Efficient Gene Regulatory Strategy

 Kristopher J. Kennedy,<sup>a</sup> Florian J. Widner,<sup>a</sup> Olga M. Sokolovskaya,<sup>a\*</sup> Lina V. Innocent,<sup>a</sup> Rebecca R. Procknow,<sup>a</sup>  Kenny C. Mok,<sup>a</sup>  Michiko E. Taga<sup>a</sup>

<sup>a</sup>Department of Plant and Microbial Biology, University of California, Berkeley, Berkeley, California, USA

**ABSTRACT** In bacteria, many essential metabolic processes are controlled by riboswitches, gene regulatory RNAs that directly bind and detect metabolites. Highly specific effector binding enables riboswitches to respond to a single biologically relevant metabolite. Cobalamin riboswitches are a potential exception because over a dozen chemically similar but functionally distinct cobalamin variants (corrinoid cofactors) exist in nature. Here, we measured cobalamin riboswitch activity *in vivo* using a *Bacillus subtilis* fluorescent reporter system and found, among 38 tested riboswitches, a subset responded to corrinoids promiscuously, while others were semiselective. Analyses of chimeric riboswitches and structural models indicate, unlike other riboswitch classes, cobalamin riboswitches indirectly differentiate among corrinoids by sensing differences in their structural conformation. This regulatory strategy aligns riboswitch-corrinoid specificity with cellular corrinoid requirements in a *B. subtilis* model. Thus, bacteria can employ broadly sensitive riboswitches to cope with the chemical diversity of essential metabolites.

**IMPORTANCE** Some bacterial mRNAs contain a region called a riboswitch which controls gene expression by binding to a metabolite in the cell. Typically, riboswitches sense and respond to a limited range of cellular metabolites, often just one type. In this work, we found the cobalamin (vitamin B<sub>12</sub>) riboswitch class is an exception, capable of sensing and responding to multiple variants of B<sub>12</sub>—collectively called corrinoids. We found cobalamin riboswitches vary in corrinoid specificity with some riboswitches responding to each of the corrinoids we tested, while others responding only to a subset of corrinoids. Our results suggest the latter class of riboswitches sense intrinsic conformational differences among corrinoids in order to support the corrinoid-specific needs of the cell. These findings provide insight into how bacteria sense and respond to an exceptionally diverse, often essential set of enzyme cofactors.

**KEYWORDS** *Bacillus subtilis*, RNA biology, cobalamin, coenzyme, cofactor, corrinoid, gene regulation, metabolism, physiology, riboswitch, vitamin B<sub>12</sub>

Controlling gene expression is an essential task cells accomplish in a variety of ways. Noncoding RNAs are one such means of gene regulation, acting in parallel or in concert with historically better-studied protein-based mechanisms (1). In bacteria and archaea, riboswitches are a widespread type of gene regulatory RNA with the distinct ability to sense particular intracellular metabolites by direct binding (2). These RNAs are typically located in the 5'-untranslated region of mRNA transcripts and function as cis-regulators of downstream genes within their transcripts. A riboswitch is composed of an effector-binding aptamer domain and an expression platform. The aptamer domain adopts a three-dimensional (3D) structure that can bind its cognate effector molecule. The expression platform domain is a regulatory switch that interprets the effector-binding state of the upstream aptamer typically to promote or disrupt the transcription or translation of downstream genes (3). The diversity of riboswitch effectors and regulatory mechanisms

**Editor** Gisela Storz, National Institute of Child Health and Human Development (NICHD)

**Copyright** © 2022 Kennedy et al. This is an open-access article distributed under the terms of the [Creative Commons Attribution 4.0 International license](https://creativecommons.org/licenses/by/4.0/).

Address correspondence to Michiko E. Taga, taga@berkeley.edu.

\*Present address: Olga M. Sokolovskaya, Department of Infectious Diseases, Genentech Inc., 1 DNA Way, South San Francisco, CA, 94080, USA.

The authors declare no conflict of interest.

**Received** 27 April 2022

**Accepted** 25 July 2022

**Published** 22 August 2022

has revealed fundamental insights into how bacteria sense and respond to dynamic environments and has also driven new approaches for precise control and manipulation of microbes for human purposes (4–7).

Cobalamin (Cbl) riboswitches (also called “B<sub>12</sub> riboswitches” or “adenosylcobalamin riboswitches”) are among the most widespread and structurally diverse types of riboswitch in bacteria (8). They directly bind various forms of the enzyme cofactor Cbl as a cognate effector (Fig. 1A and C) (9) to regulate genes involved in the biosynthesis, transport, and usage of Cbl. Cbl-dependent enzymes function in common metabolic pathways, including methionine synthesis, deoxyribonucleotide synthesis, tRNA modification, and the degradation of certain amino acids, fatty acids, and biopolymers (10–23). Cbl is also required for rarer metabolic processes involved in antibiotic synthesis, mercury methylation, catabolism of steroids, and many others (24–37). Comparative genomic studies indicate most bacteria perform Cbl-dependent metabolism and Cbl-riboswitches often regulate these processes (8, 38, 39). However, an overlooked facet among most riboswitch studies is that Cbl is just one member of a class of enzyme cofactors known as corrinoids (Fig. 1B) (40). In fact, Cbl-dependent enzymes in bacteria often function with corrinoids other than Cbl. Yet, it remains unclear whether the dozens of naturally occurring corrinoid cofactors are also Cbl-riboswitch effectors (41–47).

Corrinoid cofactors contain a highly substituted corrin ring with a central cobalt ion, a variable “upper ligand” moiety coordinating the  $\beta$  axial face of the cobalt, and a tail structure extending from the corrin ring and terminating in a variable “lower ligand” moiety that often coordinates the  $\alpha$  axial face of the cobalt (Fig. 1A and B). The molecular basis of selectivity of Cbl-riboswitches for upper ligand variants of Cbl has been relatively well studied, but selectivity for corrinoid tail variants remains mostly unexplored (9, 48, 49). To our knowledge, only one study has directly examined corrinoid tail specificity of a single Cbl-riboswitch. *In vitro* binding measurements showed the aptamer of the *Escherichia coli* *btuB* Cbl-riboswitch binds the complete corrinoids Cbl and 2-methyladeninylcobamide ([2-MeAde]Cba) with a 3.2-fold difference in affinity ( $K_D = 89$  and 290 nM, respectively). Furthermore, cobinamide (Cbi), an incomplete corrinoid with a truncated tail, binds the aptamer with roughly 8,000-fold lower affinity than Cbl ( $K_D = 753 \mu\text{M}$ ), suggesting this aptamer binds corrinoids in a selective manner (50). In light of these previous studies of corrinoid-specific metabolisms and Cbl-riboswitches, we hypothesize Cbl-riboswitches harbor a range of distinct corrinoid tail-specific activities.

Here, we examined how a panel of 38 Cbl-riboswitches derived from 12 bacterial species responds to the distinct tail structures of four corrinoids: Cbl, pCbl, and CreCba, representatives of the benzimidazolyl, purinyl, and phenolyl cobamides, respectively, and Cbi, an incomplete corrinoid (Fig. 1B). To compare activities among several dozen Cbl-riboswitches, we devised a live cell fluorescence-based reporter system in *Bacillus subtilis*. In contrast to conventional *in vitro* biochemical approaches, this riboswitch reporter system captures the complete corrinoid-responsive gene regulatory process and provides rapid functional measurements with multiple effectors in parallel. Our results obtained from experiments in the reporter system in conjunction with comparative structural analyses of Cbl-riboswitches and corrinoid effectors allowed us to develop a mechanistic model for how corrinoid tail-specific gene regulation is achieved. Additionally, we examine a gene regulatory strategy for the corrinoid specificity of a Cbl-riboswitch and discuss the conceptual and practical implications of these findings.

## RESULTS

**Experimental strategy—development of an *in vivo* reporter system.** In order to compare corrinoid selectivity among several Cbl-riboswitches and corrinoids, we constructed an *in vivo* green fluorescent protein (GFP) reporter system. We initially attempted to use an *E. coli* host for the reporter system but found most of the riboswitches we tested did not function in the *E. coli* host. We chose *B. subtilis* as an alternative host organism because of the robust genome engineering and gene expression toolsets available. Furthermore, the *B. subtilis* genome does not contain any annotated corrinoid biosynthesis or remodeling

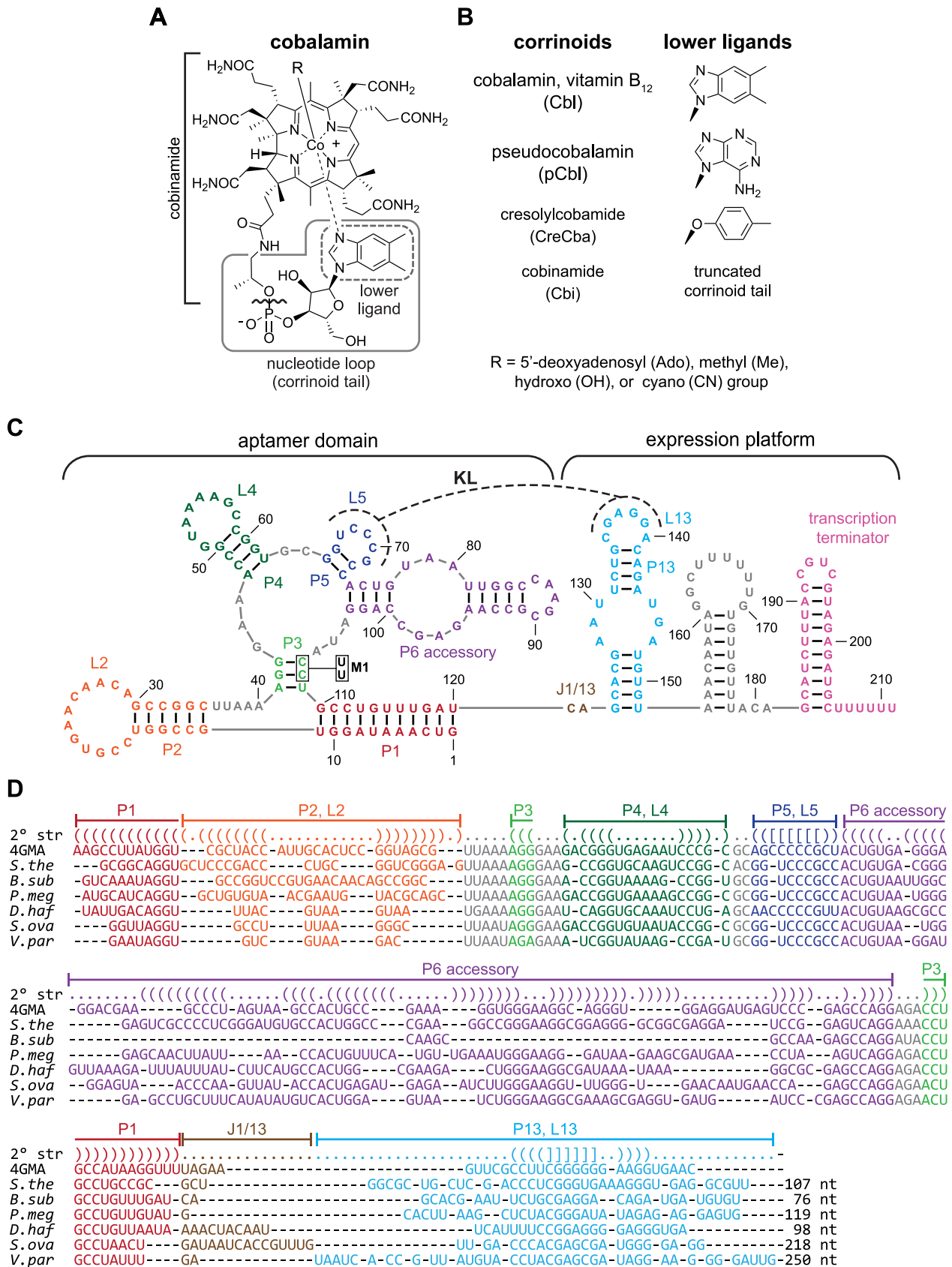


**FIG 1** Main corrinooids and riboswitches examined in this study. (A) Chemical structure of cobalamin, also called vitamin B<sub>12</sub>. The gray solid line delineates the corrinoid tail region, which contains the variable lower ligand group in the gray dashed-line box. The R group is the upper ligand. (B) (Continued on next page)

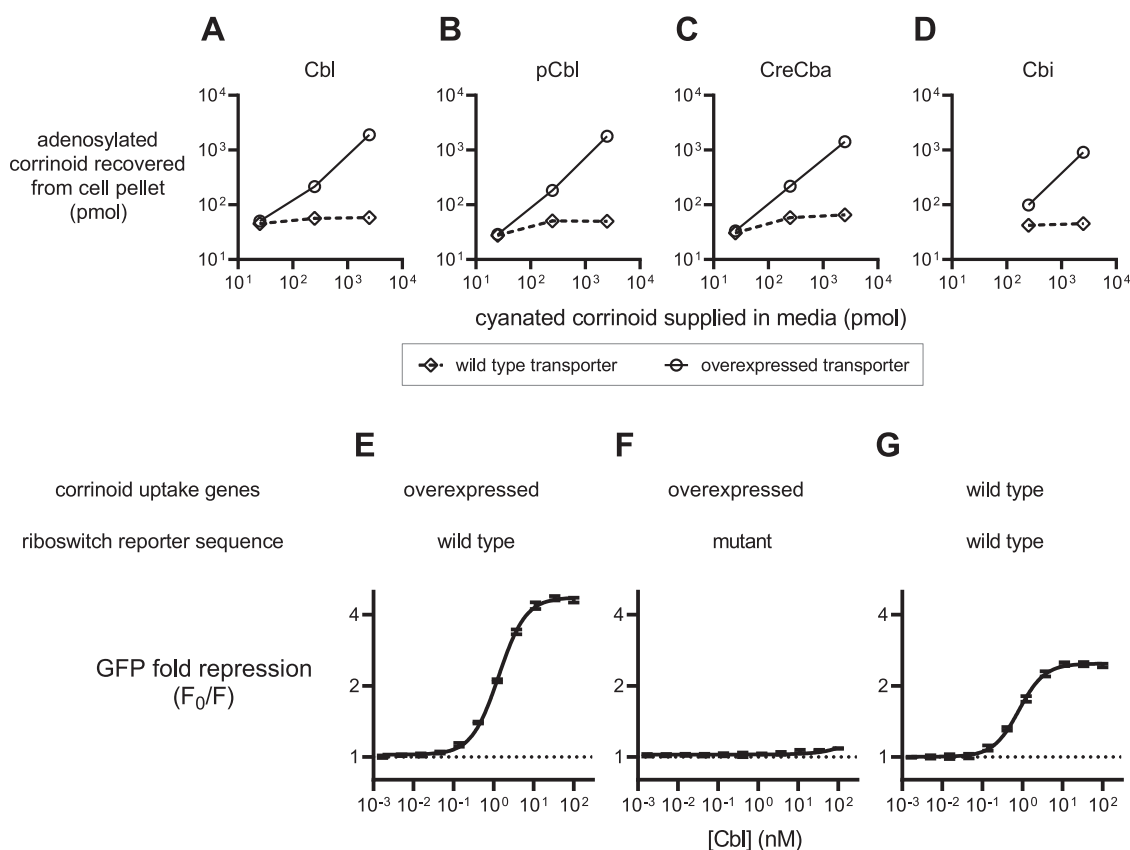


**FIG 2** Characterization of a live cell Cbl-riboswitch reporter system. (A to D) Intracellular accumulation of corrinoids in *Bacillus subtilis* strains containing the wild type (diamonds) or constitutively overexpressed (circles) corrinoid uptake genes *btuFCDR*. (E to G) Dose responses of *B. subtilis* *btuF* GFP riboswitch reporters. “Mutant” riboswitch refers to the M1 mutant version of the *B. subtilis* *btuF* riboswitch (Fig. 1C). Data points in panels A to D represent single measurements from one representative experiment. Data points and error bars in panels E to G represent mean and standard deviation of four independent replicates, and horizontal dotted lines demarcate no change in expression.

genes that would potentially interfere with a riboswitch reporter assay. We engineered the strain to overexpress the Cbl uptake and adenosylation operon, *btuFCDR*, and deleted *queG*, which encodes the only Cbl-dependent enzyme in the genome. We found *btuFCDR* overexpression increased uptake of not only Cbl, but also pCbl, CreCba, and Cbi (Fig. 2A to D). Additionally, each corrinoid was transformed from the cyanated to adenosylated form, suggesting the corrinoids are internalized to the cytoplasm, and not simply accumulating on the outer cell surface. This strain is effective for measuring the response of the *B. subtilis* *btuF* Cbl-riboswitch to a broad range of concentrations of Cbl (Fig. 2E to G). Notably, deletion of *btuR*, which encodes the adenosyltransferase that installs the Ado upper ligand group, rendered the *B. subtilis* *btuF* Cbl-riboswitch reporter insensitive to exogenously supplied CNCbl, MeCbl, and OHCbl, while retaining dose-dependent repression

#### FIG 1 Legend (Continued)

Names, lower ligand structures, and abbreviations of the corrinoids used throughout this study. Cbl, pCbl, and CreCba are “complete corrinoids” (cobamides). Cbi is an “incomplete corrinoid” that lacks the phosphoribosyl and lower ligand groups as indicated by the bracket and wavy line in the corrinoid tail in panel A. (C) Secondary structural model of the Cbl-riboswitch upstream of *B. subtilis* *btuF*. Base paired stems (P), loops (L), and junctions (J) are labeled. The P6 accessory region is highly variable in length and number of stems across Cbl-riboswitch sequences, often containing up to six paired regions. In this example, P6 accessory consists of only two paired regions. A kissing loop interaction (KL, dashed line) occurs between L5 of the aptamer and L13 of the expression platform. M1 indicates mutations C107U and C108U, which are examined in Fig. 2F. (D) Secondary structural alignments of seven representative Cbl-riboswitches examined in this study. Row “2° str” indicates paired bases as parentheses, loops, and junctions as periods, and kissing loop base pairs by brackets. PDB numbers or abbreviations are given for riboswitches from the following organisms and genes: 4GMA, *Thermoanaerobacter tengcongensis*; S. the, *Symbiobacterium thermophilum* *cblS*; B. sub, *B. subtilis* *btuF*; P. meg, *Priestia megaterium* *metE*; D. haf, *Desulfitobacterium hafniense* DSY0087; S. ova, *Sporomusa ovata* *btuB2*; V. par, *Veillonella parvula* *mutA*. Nonconserved sequences between P13 and the start codon are indicated by nucleotide sequence length (nt), but the actual sequences were omitted for clarity.

in response to AdoCbl (Fig. S1). This strongly suggests the *B. subtilis* *btuF* Cbl-riboswitch only responds to Cbl containing the 5'-deoxyadenosine upper ligand, in contrast with a report suggesting this riboswitch aptamer can also bind MeCbl and OHcbl (51).

**Comparison of corrinoid specificity among Cbl-riboswitches.** In the strain background described above, we constructed 86 reporter strains to examine riboswitches from 20 bacterial species, including 10 species known to produce or require specific corrinoids. Of the 86 reporters, 38 repressed GFP expression 0.5-fold or greater in response to one or more corrinoids. Thirty-seven of these 38 functional riboswitch expression platforms contain a predicted intrinsic transcriptional terminator suggesting they are transcriptional riboswitches. We observed extensive variation in sequence length and nucleotide composition throughout the aptamers and expression platforms of the 38 riboswitches that were functional in *B. subtilis* (Fig. 1D). Nine of the functional riboswitches are from *Priestia* (formerly *Bacillus*) *megaterium*, which produces Cbl (41), and 12 are from *Sporomusa ovata* and *Veillonella parvula* which both produce CreCba (44, 45, 52, 53). These results show Cbl-riboswitches of diverse sequence composition and origin can be examined with the *in vivo* reporter system. To address whether Cbl-riboswitches are corrinoid selective, and how corrinoid selectivity varies among Cbl-riboswitches, we measured the dose responses of the 38 functional Cbl-riboswitches to four corrinoids, Cbl, pCbl, CreCba, and Cbi. Our results show all of the riboswitches responded to more than one corrinoid, and a subset responded to all four (Fig. 3). Strikingly, all of the tested riboswitches are either semiselective (responding to more than one corrinoid) or promiscuous (responding to all four corrinoids) (Fig. 3A and B). We did not find any highly selective riboswitches that respond to only one corrinoid. The semiselective and promiscuous riboswitches all respond to Cbl and pCbl (Fig. 3C), and the promiscuous riboswitches additionally respond to Cbi and CreCba (Fig. 3D and E, points above the horizontal dashed line). Furthermore, the semiselective riboswitches are generally more sensitive to Cbl than to pCbl, while the promiscuous riboswitches respond similarly to these two corrinoids. Almost all of the riboswitches respond weakly to CreCba compared with the other three corrinoids (Fig. S2A to C). In general, corrinoid selectivity of a riboswitch appears to be associated with its taxonomic origin (Fig. 3C to E). The riboswitches from the Bacilli class are exclusively semiselective (Fig. S2A), whereas those from Negativicutes are predominantly promiscuous (Fig. S2B). The *S. ovata* *cobT* riboswitch is a notable exception discussed later. In contrast to taxonomy, corrinoid selectivity of a riboswitch is not strongly associated with the function of its regulatory target genes (Fig. S3).

Next, we attempted to identify the RNA sequence features that underlie corrinoid selectivity. Chimeric fusions of the semiselective *P. megaterium* *metE* riboswitch and the promiscuous *V. parvula* *mutA* riboswitch enabled us to examine the effects of specific domain and subdomain sequences on corrinoid selectivity (Fig. S4). Fusing the *P. megaterium* *metE* aptamer domain to the expression platform of the *V. parvula* *mutA* riboswitch produced a semiselective riboswitch chimera, while the reciprocal chimera was promiscuous, suggesting the aptamer domain is a major determinant of corrinoid selectivity (Fig. S4A). However, results from aptamer subdomain swaps of stem P1, stem-loop P2-L2, stem-loop P4-L4, and P6 accessory region were less conclusive. In the context of the *P. megaterium* *metE* riboswitch scaffold, swapping stem-loop P2-L2 or the P6 accessory region with the corresponding structures of the *V. parvula* *mutA* riboswitch produced chimeras that are less selective by gaining sensitivity to Cbi and CreCba (Fig. S4B). This suggests that these subdomains confer corrinoid promiscuity. Yet, within the *V. parvula* *mutA* riboswitch scaffold, swapping stem P1 increased corrinoid selectivity by retaining sensitivity to Cbl and pCbl, but losing sensitivity to CreCba and Cbi (Fig. S4C). The remaining chimeras partially or completely lost overall activity. These results demonstrate subdomains distributed throughout the aptamer domain may impact corrinoid selectivity; no single conserved substructure completely controls corrinoid selectivity, nor did any single structure fully convert a riboswitch's corrinoid

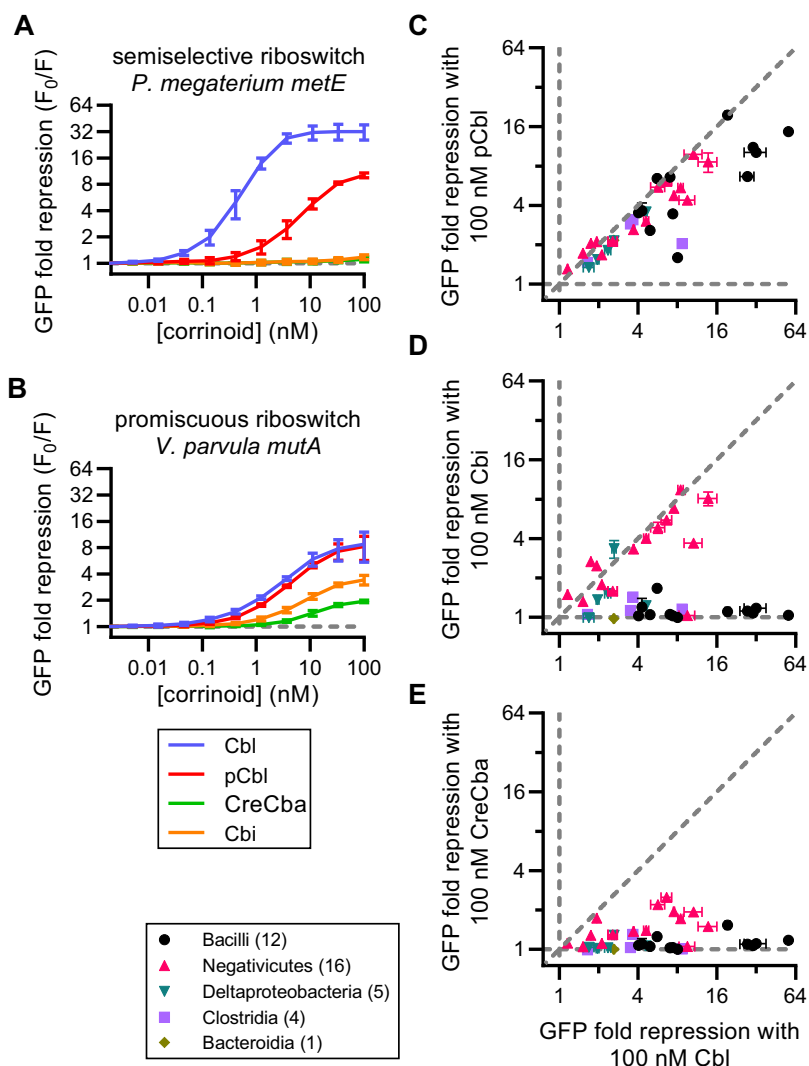


**FIG 3** Corrinoid specificity among 38 Cbl-riboswitches. (A, B) Corrinoid dose responses of two riboswitch reporter strains with distinct corrinoid specificities, representing the semiselective (A) and promiscuous (B) types. (C to E) Pairwise comparisons of GFP fold repression induced by 100 nM Cbl versus (C) pCbl, (D) Cbi, and (E) CreCba. Data points are colored by taxonomic class with the number of riboswitches analyzed from each class indicated in parentheses. Vertical and horizontal gray dashed lines demarcate a response to only one of the two corrinoids. Diagonal line demarcates equal response to two corrinoids. Data points and error bars in panels A and B represent mean and standard deviation of 10 experiments for *P. megaterium metE* and six experiments for *V. parvula mutA*. Data points and error bars in panels C to E represent mean and range of at least two independent experiments for each riboswitch.

selectivity. Thus, the source of the corrinoid selectivity phenotype appears to be complex and requires inputs from multiple subdomains of the aptamer.

**Corrinoid tail structure impacts selectivity of Cbl-riboswitches.** We next sought to identify how structural differences in the corrinoid tail affect the response of semiselective Cbl-riboswitches to corrinoids. There are no predicted hydrogen bond interactions between the lower ligand and the RNA in the X-ray crystal structures of Cbl-bound riboswitches, making it difficult to surmise how a Cbl-riboswitch might distinguish between corrinoids (51, 54, 55). Could the overall structural conformation of the corrinoid, rather than specific interactions between the RNA and the corrinoid tail, influence Cbl-riboswitch activity?

Corrinoids undergo major conformational changes when spontaneously switching between two distinct states known as “base-on” and “base-off” (56, 57). In the base-on state, a nitrogen atom in the lower ligand base is coordinated to the central cobalt

atom of the corrin ring (as shown in Fig. 1A). In the base-off state, the lower ligand base is decoordinated, allowing the tail to move more freely (58, 59). Benzimidazolyl and purinyl cobamides (e.g., Cbl, pCbl) can switch between base-on and base-off states. However, the tail moieties of phenolyl cobamides (e.g., CreCba) and Cbi cannot coordinate cobalt; therefore, these corrinoids exist exclusively in a decoordinated state (52). Interestingly, we noticed the semiselective riboswitches respond strongly to Cbl and pCbl, but weakly to Cbi and CreCba. We also observe semiselective Cbl-riboswitches are most sensitive to Cbl, which forms the base-on state more readily than pCbl (Fig. 3C; Fig. S2) (58, 59). In line with these results, the *E. coli* *btuB* riboswitch aptamer was previously shown to bind Cbl with higher affinity than Cbi and [2-MeAde]Cba (a primarily base-off corrinoid) (50). Also, all six X-ray crystal structures of Cbl-riboswitches contain Cbl in the base-on state (51, 54, 55). Based on these observations, we hypothesized that semiselective riboswitches distinguish between base-on and base-off states of corrinoids. We therefore used a range of corrinoids with diverse lower ligand structures to test whether the activity of Cbl-riboswitches quantitatively correlates with the base-on tendency of corrinoids.

We selected a panel of 16 corrinoids for this analysis, including both natural and synthetic benzimidazolyl, purinyl, and azabenzimidazolyl corrinoids. These corrinoids span a range of base-on tendency between that of Cbl and pCbl, which we measured as the ratio of spectral absorbance at 525 and 458 nm in the adenosylated form (Fig. 4A; Fig. S5). Base-on/base-off equilibrium constants for AdoCbl, Ado[2-MeAde]Cba, and pCbl in aqueous conditions have been reported as 76, 0.48, and 0.30, respectively, and are consistent with our measurements of corrinoid base-on tendency (58, 59). We observed a strong association between base-on tendency and riboswitch response in semiselective riboswitches (Fig. 4B). Even among promiscuous Cbl-riboswitches, we observe measurable sensitivity to base-on tendency, albeit to a much smaller degree (Fig. 4C). These results support the hypothesis that Cbl-riboswitches selectively respond to corrinoids by distinguishing between the base-on and base-off states of corrinoids.

**Structural comparisons between base-on and base-off tail orientations.** The results presented above led us to speculate about how a Cbl-riboswitch could detect the base-on and base-off state of a corrinoid. In all published X-ray crystal structures of Cbl-riboswitches, aptamer-effector binding is achieved mainly through van der Waals forces and shape complementarity between the binding site and base-on Cbl. Only a few hydrogen bonds between the RNA and corrinoid are observed, none of which occur with the lower ligand group of Cbl (51, 54, 55). Thus, it appears unlikely the riboswitch is directly detecting the specific chemical differences among corrinoid lower ligands. Instead, we considered whether the riboswitch discriminates base-on and base-off forms of a corrinoid by sensing corrinoid conformation. In the base-on state, the tail is spatially constrained due to the Co-N coordinate bond, whereas in the base-off form it is able to sample a wider range of spatial positions (60). To develop mechanistic insight into how the base-on and base-off states a corrinoid could impact Cbl-riboswitch activity, we leveraged the plethora of publicly accessible X-ray crystal structures of macromolecule-bound Cbl (37, 51, 54, 55, 61–70). We first assessed the range of structural conformations that are potentially sampled by corrinoids as they dynamically switch between base-on and base-off states by aligning and visually comparing various structural models of Cbl. Six base-on Cbl models were obtained from structural studies of Cbl-riboswitches and synthetic Cbl RNA aptamers, whereas base-off/His-on Cbl models were obtained from X-ray crystal structures of 10 Cbl-dependent enzymes (Table S2). After aligning and superimposing these molecular models by their central cobalt and coordinating nitrogen atoms, we observed the corrin rings and their amide and methyl substituents occupy similar spatial positions, but the tails of base-on and base-off Cbl structures occupy distinct positions (Fig. 5A and B). Moreover, the base-on Cbl tails appear in very similar positions with lower ligands in close proximity to the central cobalt ion, whereas the base-off Cbl tails appear more scattered with lower ligands more distal to the cobalt ion. These

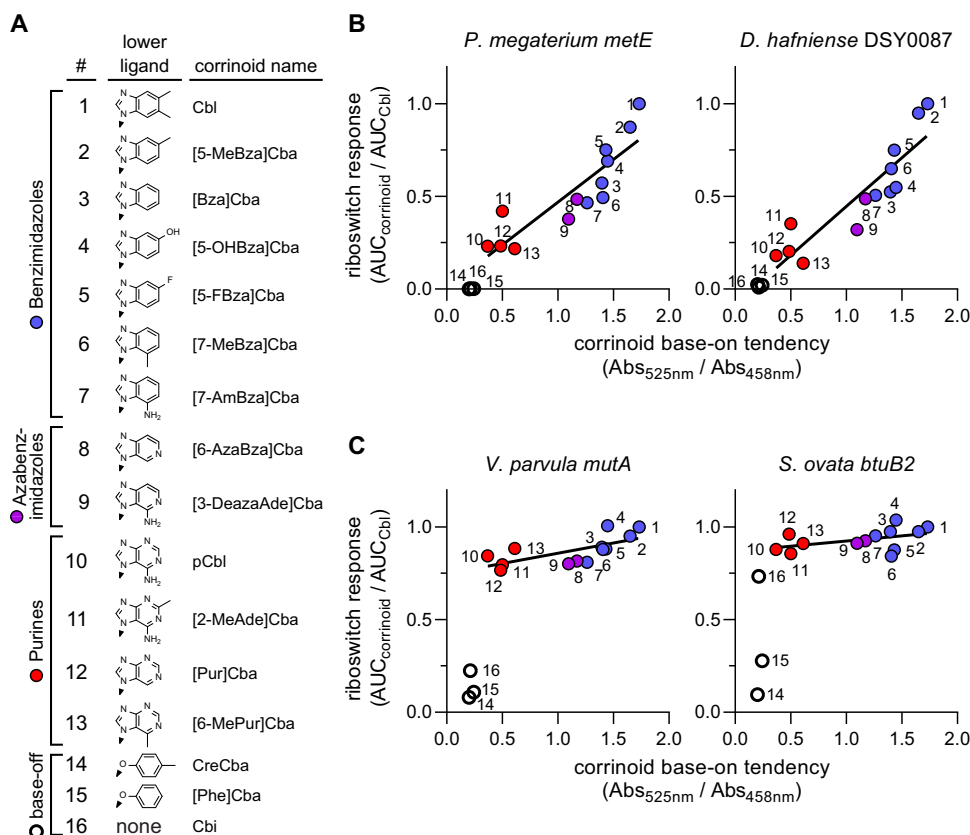


**FIG 4** Corrinoid base-on tendency correlates with corrinoid potency. (A) Sixteen adenosylated corrinoids used to test the relationship between corrinoid base-on tendency and corrinoid potency. (B) Semiselective riboswitches *P. megaterium metE* and *D. hafniense* DSY0087 and (C) promiscuous riboswitches *V. parvula mutA* and *S. ovata btuB2* were used to measure the response to each corrinoid. Base-on tendency was measured as the ratio between spectral absorbance at 525 and 458 nm in a pH 7.3 solution. Absorbance spectra are displayed in Fig. S5. The cumulative corrinoid response was measured as the area under the dose-response curve of the riboswitch reporter strain for that corrinoid (AUC<sub>corrinoide</sub>) relative to its dose response to Cbl (AUC<sub>Cbl</sub>). Corrinoids with benzimidazole (blue circles), azabenzimidazole (purple circles), and purine (red circles) lower ligands can adopt the base-on conformation. The corrinoids that are unable to adopt the base-on state (CreCba, [Phe]Cba and Cbi) are represented by empty circles. Trendlines in B and C were fit to data points of corrinoids with benzimidazole, azabenzimidazole, and purine lower ligands, with strictly base-off corrinoids excluded. Each data point represents a single measurement of riboswitch dose-response and corrinoid base-on tendency.

structural alignments visually convey the degree to which the conformations of base-on and base-off corrinoids can vary among biomolecular complexes.

Next, we compared the positions of the aligned base-on and base-off Cbl models in the context of 3D Cbl-riboswitch models. We analyzed X-ray crystal structures of the two Cbl-riboswitches that contain resolved kissing loop structures: one from *Thermoanaerobacter tengcongensis* (Fig. 5C and D) and one identified from a marine metagenome sequence (Fig. S6A and B) (54). These structural models show the base-on tails are contained within the binding site, whereas the tails of the base-off Cbl structures protrude away from the binding site and clash with the L5-L13 kissing loop. Although the *B. subtilis btuF* (Fig. S6C and D) and *Symbiobacterium thermophilum cbtI* (Fig. S6E and F) riboswitch models do not contain the L13 structure of the kissing loop, some of the modeled base-off tails clash with L5 of the aptamer in these structures (51, 55). The kissing loop has been shown to play a key mechanistic role of sensing the corrinoid-binding state of the aptamer domain to influence downstream regulatory structures in the expression platform (71, 72). If kissing loop formation in semiselective Cbl-riboswitches is sensitive to the base-on and base-off states of the corrinoid, then corrinoid selectivity may be mediated by either selective binding by the aptamer or selective formation of downstream regulatory structures.

To determine whether the expression platform structures can impact corrinoid



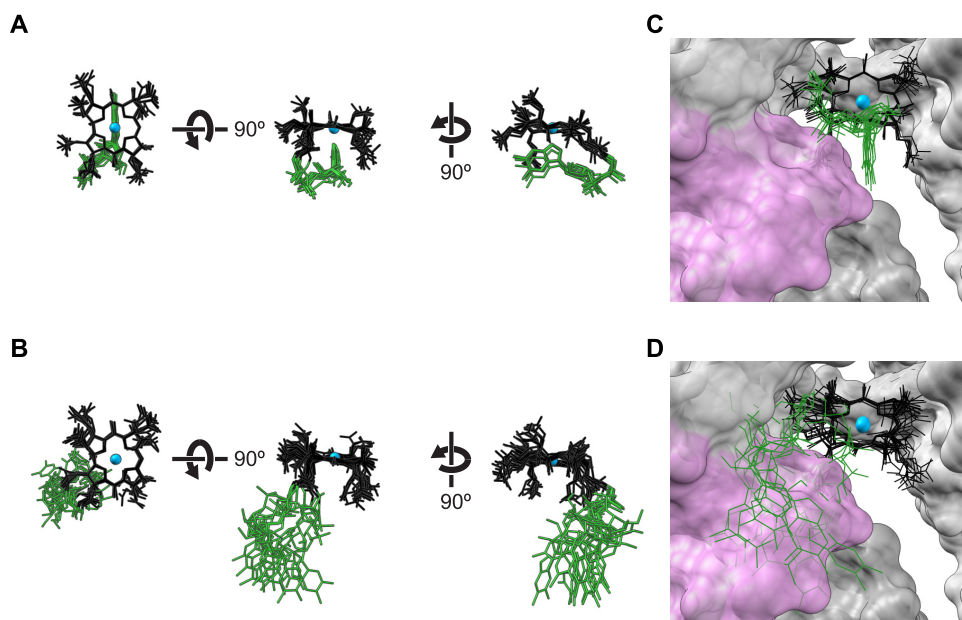


**FIG 5** Distinct tail positions among base-on and base-off corrinoids may impact binding of corrinoids to riboswitches. 3D alignments of Cbl structural models derived from published X-ray crystal structures of (A) base-on Cbl in complex with RNAs and (B) base-off Cbl in complex with proteins. The Cbl-binding site in the X-ray crystal structure of the *Thermoanaerobacter tengcongensis* Cbl-riboswitch (PDB ID 4GMA) is depicted with (C) base-on and (D) base-off Cbl alignments. Cbl models were aligned by the cobalt and coordinating nitrogen atoms in the corrin ring. Structures of the corrin ring, cobalt, and tail of Cbl are colored in black, blue, and green, respectively. Upper ligand structures of Cbl were omitted for clarity. Riboswitch RNA structures are depicted as space-filled models with the L5-L13 kissing loop in pink and the rest of the RNA in gray.

selectivity, we examined corrinoid-selective binding separately from subsequent corrinoid-selective regulation. We tested for promiscuous binding by comparing the Cbl dose response of the *P. megaterium metE* Cbl-riboswitch in the presence and absence of competing 100 nM Cbi and found the response to Cbl is unaffected by Cbi (Fig. S7A and B). This indicates Cbi does not compete with Cbl for riboswitch binding, supporting corrinoid-selective binding as the mechanism of semiselectivity. However, when the aptamer of this semiselective riboswitch is replaced with the aptamer of the promiscuous *S. ovata nika* riboswitch, it retains semiselectivity, suggesting the *P. megaterium* expression platform also plays a role in corrinoid selectivity (Fig. S7A). Interestingly, the Cbl dose response of the *S. ovata nika/P. megaterium metE* chimeric riboswitch does become sensitized to competing Cbi addition, confirming the *S. ovata nika* aptamer retains sensitivity to base-off corrinoid in the context of this chimera (Fig. S7C). Taken together, these results show base-off corrinoids may impede both Cbl-riboswitch binding and formation of regulatory structures, explaining the link between corrinoid base-on tendency and riboswitch activity observed in Fig. 4.

**Gene regulatory strategy of corrinoid selectivity.** While the prior experiments clearly demonstrate Cbl-riboswitches are capable of distinguishing between corrinoids, we wondered what purpose Cbl-riboswitch corrinoid selectivity might serve in the organisms containing these regulatory systems. We posit Cbl-riboswitch selectivity reflects a regulatory strategy that complements the corrinoid-specific requirements of the cell and avoids gene mis-regulation. As a specific example, we hypothesize only corrinoids that are functionally compatible with a Cbl-dependent enzyme should cause riboswitch-mediated repression of the expression of its Cbl-independent counterpart (Fig. 6A and B). We tested this hypothesis directly in *B. subtilis* by examining the function and regulation of methionine synthase isozymes MetE (Cbl-independent) and MetH (Cbl-dependent). In bacterial genomes with both *metE* and *metH*, an *S*-adenosyl methionine (SAM) riboswitch fused in tandem with a Cbl-riboswitch is commonly found upstream of

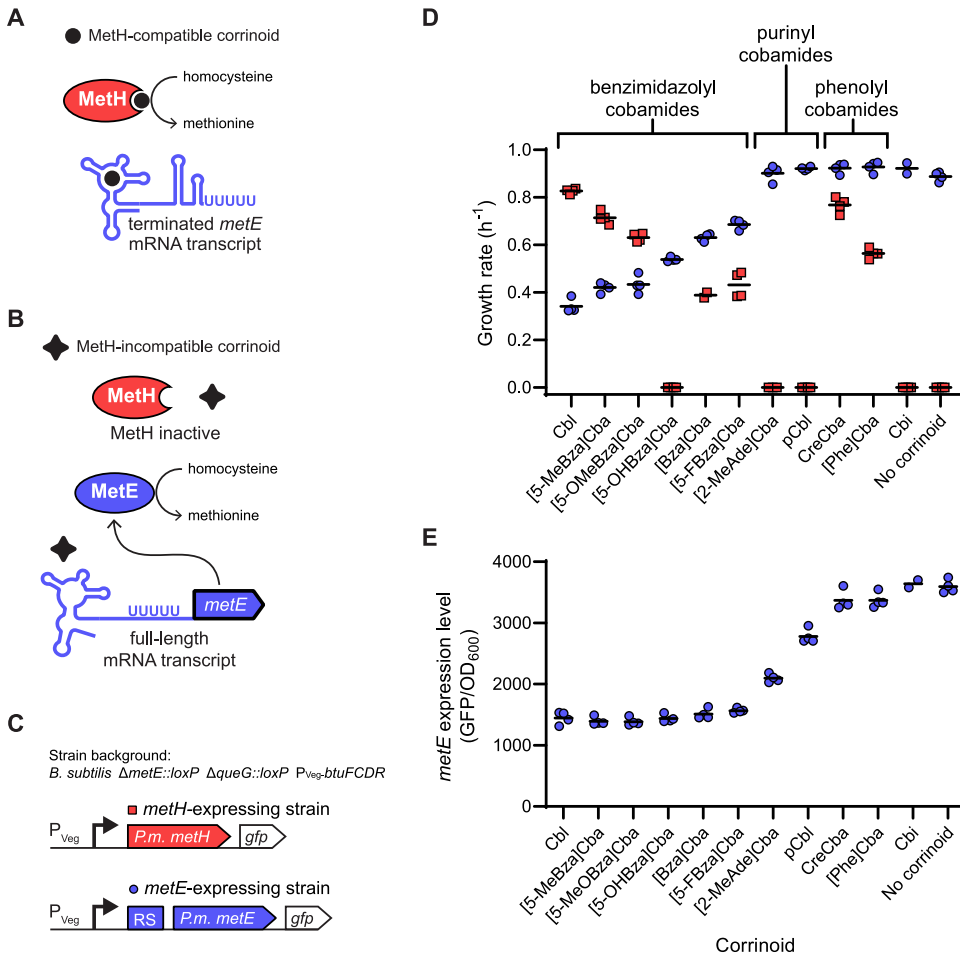


**FIG 6** Corrinoid specificities of the *P. megaterium* *metE* riboswitch and *P. megaterium* MetH enzyme are aligned. Expression of the Cbl-independent methionine synthase MetE and enzymatic activity of the Cbl-dependent methionine synthase MethH are potentially impacted by the presence of (A) Meth-compatible corrinoids and (B) Meth-incompatible corrinoids. (C) The *metH*-expressing strain (red) is a *B. subtilis*  $\Delta metE::loxP \Delta queG::loxP P_{veg}\text{-}btuFCDR$  strain heterologously expressing *P. megaterium* *metH*. The *metE*-expressing strain (blue) is a *B. subtilis*  $\Delta metE::loxP \Delta queG::loxP P_{veg}\text{-}btuFCDR$  strain heterologously expressing *P. megaterium* *metE* downstream from a SAM-Cbl tandem riboswitch (RS). Each methionine synthase gene is constitutively expressed from the  $P_{veg}$  promoter and is transcriptionally fused to *gfp*. (D) Growth rates of the *metE*-expressing strain (blue circles) and *metH*-expressing strain (red squares) were measured in methionine-dependent culture conditions containing 20 nM corrinoid. (E) Expression of *metE* was measured as GFP fluorescence per OD<sub>600</sub> in medium lacking methionine, supplemented with 20 nM corrinoid. Data points are individual measurements and black horizontal lines represent the mean of the four replicate measurements.

the *metE* gene (73, 74). The *B. subtilis* genome contains *metE* but lacks *metH*, and no Cbl-riboswitch is located upstream of *metE*. We, therefore, constructed strains of *B. subtilis* that heterologously express the *metE* or *metH* locus from the Cbl-producing species *P. megaterium*, in a  $\Delta metE$  background with overexpressed corrinoid uptake genes (Fig. 6C) (75–77). In each strain, the *P. megaterium* genes are constitutively transcribed from the promoter  $P_{veg}$  and also contain a transcriptionally fused *gfp* to measure expression levels. Growth of the *B. subtilis* strain expressing *P. megaterium* *metH* in a medium lacking methionine was supported to various extents by most benzimidazolyl and both phenolyl cobamides, but not by [5-OHBza]Cba, the purinyl cobamides, or Cbi (Fig. 6D, red squares). This result indicates Meth-dependent growth is influenced by the corrinoid tail structure, as observed previously in other bacteria (78–82). In the *B. subtilis* strain containing the *P. megaterium* *metE* locus which includes the repressing SAM-Cbl-riboswitch, growth was suppressed by benzimidazolyl cobamides to different extents (Fig. 6D, blue circles). This growth pattern coincides with the GFP repression measured for the *metE* riboswitch (Fig. 6E), except that

the repression of *metE* by purinyl cobamides is apparently insufficient to suppress growth in this context. Comparison of the two strains in response to a suite of corrinoids reveals a striking correspondence between riboswitch-mediated suppression of growth in the *metE*-containing strain and growth promotion by corrinoids in the *metH*-containing strain (Fig. 6C). [5-OHBza]Cba and the phenolyl cobamides are exceptions to the trend, though in neither case is MetE-dependent growth completely suppressed by a corrinoid incompatible with MetH. This result demonstrates riboswitch-based repression and cobalamin-dependent isozyme function are largely aligned for the *P. megaterium metE-metH* pair and suggests that Cbl-riboswitch specificity may generally adhere to a regulatory strategy reflecting the cell's corrinoid preference.

## DISCUSSION

Riboswitches are key regulators of microbial gene expression. The Cbl-riboswitch was the first type discovered and is among the most widely distributed riboswitch classes in bacteria and archaea (9, 83). Previous biochemical and structural studies have uncovered the major molecular features of the Cbl-riboswitch response to Cbl, including how upper ligand variants of Cbl impact their function (48, 49, 51, 54, 55, 71, 72, 74, 84). Yet few studies have examined how other naturally occurring corrinoids containing diverse lower ligand structures impact gene regulation by Cbl-riboswitches (50). Here, we found Cbl-riboswitches vary in their ability to discriminate between corrinoids, with some being semiselective on the basis of corrinoid base-on/off state, and others being promiscuous. These results were enabled by a carefully designed fluorescent reporter system capable of measuring the responses of dozens of Cbl-riboswitches to multiple corrinoids *in vivo* (Fig. 2; Fig. S1). Because several naturally occurring corrinoids other than Cbl appear to be potent effectors for Cbl-riboswitches, we propose the term “corrinoid riboswitch” be adopted to describe this broad class of RNAs more accurately. This may also mitigate the inconsistent and overlapping terminology used in the literature (i.e., cobalamin riboswitch, adenosylcobalamin riboswitch, B<sub>12</sub> riboswitch, vitamin B<sub>12</sub> riboswitch, etc.).

We can roughly estimate the intracellular corrinoid concentrations in our corrinoid dose-response experiments to assess the physiological relevance the *in vivo* Cbl-riboswitch data. Observing most of the corrinoid in the medium is imported by the *B. subtilis* riboswitch reporter cells (Fig. 2A to D), and assuming a cell volume of 10<sup>-15</sup> L and a culture cell titer of 1012 cells/L at OD<sub>600</sub> = 1, we calculate the cytoplasmic corrinoid concentrations to range from 0.01 to 100 μM in the corrinoid dose-response experiments—a 1,000-fold increase from the cell culture medium to the cytoplasm. Reports of binding affinity (*K<sub>D</sub>*) for riboswitch aptamers to AdoCbl range from 0.026 to 90 μM, which is within the range of our estimated intracellular corrinoid concentrations (48, 50, 54, 72, 85). Additionally, Cbl uptake has been measured in some bacterial species. In *E. coli*, the minimum cytoplasmic Cbl concentration to support MetH-dependent growth is roughly 0.03 μM (86). In studies of Cbl uptake across several bacterial species, saturating Cbl uptake can result in cytoplasmic Cbl concentrations in the low μM to low mM range, depending on the species (87, 88). Taken together, these data and calculations support the physiological relevance of the Cbl-riboswitch responses measured in this study.

We observed Cbl-riboswitches display different degrees of corrinoid selectivity, with some that responded to a subset of corrinoids (semiselective) while others responded to all tested corrinoids (promiscuous) (Fig. 3; Fig. S2). Our chimeric riboswitch results suggest sequence and structural determinants of corrinoid selectivity are dispersed throughout the Cbl-riboswitch aptamer scaffold rather than being confined to a single conserved region (Fig. S4). This finding contrasts with other studies of riboswitch specificity. For example, in a study of Cbl upper ligand specificity, a few key residues in the Cbl binding site were sufficient to fully convert a Cbl-riboswitch from MeCbl-specific to AdoCbl-specific (48). In purine riboswitches, effector specificity is achieved by positioning of a critical conserved uracil or cytosine residue in the binding site of the aptamer, which forms a base-pair with the adenine or guanine effector, respectively. Among the

various families of SAM riboswitches, highly specific binding of SAM and exclusion of S-adenosyl homocysteine (SAH) is achieved by RNA structures that discriminate the charged sulfonium ion of SAM from the uncharged sulfoether of SAH (89). In contrast, the SAM/SAH riboswitch class attains effector promiscuity for SAM and SAH by a general lack of interaction between the RNA and the aminocarboxypropyl side chains of these effectors (90, 91). This is reminiscent of Cbl-riboswitches which similarly have few molecular contacts between the RNA and corrinoid tail (50, 54, 55, 84).

Overall, our structural model analyses support a mechanism in which semiselective Cbl-riboswitches primarily sense the distinct corrinoid tail orientations of the base-on and base-off forms. In this case, Cbl-riboswitches only indirectly sense the chemical composition of the variable lower ligand group, with differential binding largely determined by steric effects and shape complementarity (Fig. 4 and 5). Recent molecular dynamics simulations of the *T. tengcongensis* Cbl-riboswitch suggest that the kissing loop structure may form prior to effector binding, which would place even greater constraints on the corrinoid tail orientation to achieve shape complementarity with its binding site (92). Additionally, some Cbl-riboswitches may in fact bind base-off corrinoids but disrupt subsequent formation of downstream regulatory structures of the expression platform, perhaps by interfering with the kissing loop (Fig. S7). A similar feature has been observed in tetrahydrofolate (THF) riboswitches where chemical variations in the para-aminobenzoic acid moiety of THF analogs differentially perturb expression platform structures without affecting aptamer binding (93). The mechanisms of corrinoid selectivity of Cbl-riboswitches could be directly tested in future structural or biochemical studies of promiscuous Cbl-riboswitches with base-on and base-off corrinoids.

In regard to gene regulatory strategies, it seems sensible that Cbl-riboswitches are not highly effector-specific because bacteria are often flexible in their corrinoid usage. A variety of corrinoids have been shown to support growth of *C. difficile*, *S. ovata*, and *Ensifer meliloti* despite each of these organisms displaying highly specific corrinoid production (82, 94, 95). Furthermore, because corrinoid auxotrophy is prevalent among corrinoid-dependent bacteria, many organisms may need to take advantage of the wide range of corrinoids that may be available in their environment (96). Thus, the range of effector selectivity we observe among Cbl-riboswitches may reflect a coevolution between corrinoid-responsive gene regulation and corrinoid-dependent physiology. Our result demonstrating complementary corrinoid selectivity between *P. megaterium* MetH-dependent growth and Cbl-riboswitch-dependent expression of MetE is consistent with this notion (Fig. 6).

Alternatively, the preference for base-on corrinoids among Cbl-riboswitches may function as a proxy to discriminate complete corrinoid coenzymes from incomplete corrinoids such as Cbi, which often function poorly as coenzymes. This idea has been proposed as an explanation for the remarkably high selectivity of the corrinoid uptake system in mammals (97). Interestingly, we found all but one of the *S. ovata* riboswitches tested are promiscuous types that can respond to its natively produced CreCba. The notable exception is a semiselective riboswitch upstream of the gene *cobT* (Fig. S2B), which functions in a late step of corrinoid biosynthesis that occurs after synthesis of Cbi (53, 98–103). Thus, this Cbl-riboswitch that discriminates against Cbi may allow homeostatic regulation of *cobT* in response to complete corrinoids like Cbl, while preventing unproductive repression of *cobT* in the presence of incomplete corrinoids like Cbi. Future studies examining corrinoid-specific gene regulation of riboswitches in the context of their native organisms may help clarify which regulatory strategies are generally at play in corrinoid-related bacterial physiology.

Our findings fit into a broader discussion of how corrinoids impact complex microbial communities (104). In future studies, it will be worth examining how the interplay between corrinoid-specific gene regulation and corrinoid-specific metabolic pathways influence microbial interactions. There is also significant interest in the fields of bioengineering and synthetic biology to use riboswitches as gene regulatory devices because

they act more rapidly and efficiently than protein-based regulatory systems (6, 7, 105, 106). Riboswitches have also become desirable therapeutic drug targets because they often control essential metabolic pathways in pathogenic microbes (4, 5, 107). Broader consideration of the conformational dynamics of larger types of effector molecules, including organic cofactors, antibiotics, and their analogs could aid efforts to engineer synthetic RNA-based regulatory platforms that function robustly *in vivo*. This could also inform future efforts to develop synthetic antimetabolites that, for example, elicit gene mis-regulation, instead of a more common strategy of creating inhibitors for enzymes (108, 109).

The chemical diversity of corrinoids is intrinsically linked to a vast array of metabolic processes and microbial interactions. Yet it remains unclear how microbes have evolved to cope with and thrive on the assortment of natural corrinoid analogs, especially compared with other primary metabolites, including organic cofactors, nucleotides, and amino acids which typically require one specific structural form for precise biological functions. We have gained new appreciation for the impacts of chemical diversity on biological function by focusing on the Cbl-riboswitch with its distinctively complex structure and regulatory mechanism, and by accounting for the often overlooked biological and ecological roles of corrinoid analogs. Future studies into the evolution of microbial molecular specificity for corrinoids may yield further insight into the nature of these exceptionally versatile coenzymes.

## MATERIALS AND METHODS

**Cbl-riboswitch sequence analysis.** Cbl-riboswitch sequences, chromosomal coordinates, and regulation information were downloaded from the RiboD online database (73) (Table S1). The genome of *Sporomusa ovata* was not included in the RiboD database, so we used the RiboswitchScanner webserver to search for Cbl-riboswitches in this organism (110, 111). Cbl-riboswitch aptamer sequences were manually aligned by conserved secondary structures bounded by the 5' and 3' ends of the P1 stem (8, 85) (Data Set S1). The P13-L13 stem-loop and potential intrinsic transcriptional termination hairpin structures of the expression platform were identified using secondary structure prediction tools in RNAstructure 6.2 (112, 113). Intrinsic terminators were identified as stem loops directly preceding a sequence of five or more consecutive uracil residues (114, 115). Sequence alignment and annotation was carried out in JalView 2.11.1.4 (116). Cartoons of riboswitch secondary structures were constructed using the StructureEditor program of RNAstructure 6.2 (113).

**Corrinoid production, extraction, purification, and analysis.** Cyanocobalamin, adenosylcobalamin, methylcobalamin, hydroxocobalamin, and dicyanocobinamide were purchased from MilliporeSigma. All other corrinoids used in this study were produced in bacterial cultures and purified in cyanated form as previously described (82, 95, 117, 118). For the experiments in Fig. 4 and Fig. S5, corrinoids other than cobalamin were chemically adenosylated to obtain the coenzyme (5'-deoxyadenosylated) form as previously described (82, 117).

UV/Vis spectra were collected from corrinoid samples in UV/Vis-transparent 96-well microtiter plates (greiner bio-one UV-STAR 675801) using a BioTek Synergy 2 or Tecan Infinite M1000 Pro plate reader. To measure concentrations of corrinoid stock solutions, corrinoid samples were diluted 10-fold in 10 mM sodium cyanide to obtain the dicyanated base-off form of the corrinoid. The concentration of the dicyanated corrinoid was calculated using the extinction coefficient  $\epsilon_{580} = 10.1 \text{ mM}^{-1} \text{ cm}^{-1}$  (52, 119). For adenosylated corrinoids used in Fig. 4 and Fig. S5, base-on tendency at neutral pH was measured as the ratio of spectral absorbance at 525 nm and 458 nm in phosphate-buffered saline solution pH 7.3 at 37°C (47, 59).

**Plasmid and strain construction.** Plasmids generated in this study were constructed with one-step isothermal assembly (120) and introduced into *E. coli* strain XL1-Blue by heat shock transformation. Riboswitch reporter plasmids were constructed in the shuttle vector pSG29 for single copy integration at the *amyE* locus of the *B. subtilis* chromosome (121). Riboswitch DNA sequences were inserted between the transcriptional start site of the constitutive  $P_{\text{veg}}$  promoter and the *gfp* translational start site of pSG29. For riboswitch sequences that resulted in no detectable GFP signal under any conditions, a synthetic ribosome binding site (RBS) sequence R0 (5'-GATTAATAATAAGGAGGACAAAC-3') from pSG29 was placed between the riboswitch sequence and *gfp* translational start site (Table S1B and C).

Strains used in this study are listed in Table S1A. All *B. subtilis* riboswitch fluorescent reporter strains and *B. subtilis* strains expressing *P. megaterium metE* and *metH* used in this study are derived from the high-efficiency transformation strain SCK6, which has a xylose-inducible competence gene cassette (122). Preparation of competent cells and transformations of all SCK6-derived strains were performed as previously described (122). The strain KK642, which constitutively overexpresses the corrinoid uptake genes, was constructed by deletion of gene *queG* and replacement of the promoter and 5' untranslated region of the *btuFCDR* operon with the  $P_{\text{veg}}$  promoter and R0 RBS (121). *B. subtilis* genes *queG*, *btuR*, and *metE* were targeted for deletion by recombination with kanamycin resistance cassettes containing flanking sequence homology to each respective locus. Kanamycin resistance cassettes were PCR-amplified

from genomic DNA of *B. subtilis* strains BKK08910 ( $\Delta queG::kan^R$ ), BKK33150 ( $\Delta btuR::kan^R$ ), and BKK13180 ( $\Delta metE::kan^R$ ) (123). Kanamycin resistance cassettes were removed by Cre-Lox recombination using plasmid pDR244 as previously described (123).

*B. subtilis* strains heterologously expressing *metE* and *metH* from *P. megaterium* were constructed as follows. The *metE* and *metH* genes were PCR-amplified from genomic DNA of *P. megaterium* DSM319 and cloned between the transcriptional start site and the *gfp* translational start site of pSG29. The *P. megaterium metE* amplified fragment starts at the SAM-Cbl tandem riboswitch in the 5' UTR and ends at the *metE* stop codon, whereas the *P. megaterium metH* fragment starts at the *metH* RBS, which is composed of 20 nucleotides preceding the *metH* translational start site and ends at the *metH* stop codon.

Riboswitch reporter plasmids and plasmids containing *P. megaterium metE* and *metH* were linearized by restriction enzyme digest with Scal-HF (New England Biolabs) and selected for integration at the *amyE* locus of *B. subtilis* by plating on lysogeny broth (LB) agar with 100  $\mu$ g/mL spectinomycin. Colonies were screened for integration at *amyE* by colony PCR. All stocks of bacterial strains were stored in 15% glycerol at  $-80^\circ\text{C}$ .

**Intracellular corrinoid accumulation experiments.** *B. subtilis* strains were inoculated from single colonies into 50 mL LB and grown with aeration at  $37^\circ\text{C}$  in a shaking incubator (Gyromax 737R, Amerex Instruments, Inc.) for 5 to 6 h until reaching an optical density at 600 nm ( $\text{OD}_{600}$ ) of 1.0 to 1.5. Each culture was diluted 10-fold in LB and split into 13 25-mL cultures containing 0, 25, 250, or 2500 picomoles of a cyanated corrinoid (Cbl, pCbl, CreCba, and Cbi). These cultures were incubated at  $37^\circ\text{C}$  with aeration for 3 to 4 h to a final  $\text{OD}_{600}$  of 1.5 to 2.0. The cells were pelleted by centrifugation at 4,000 g for 10 min. Cell pellets were rinsed three times by resuspension in 10 mL phosphate-buffered saline solution pH 7.3 followed by centrifugation. After the final centrifugation, tubes were wrapped in aluminum foil to protect adenosylated corrinoids from exposure to light.

To extract intracellular corrinoids, cell pellets were resuspended in 5 mL of 100% methanol by vigorous vortexing for 30 s. Samples were stored at  $-80^\circ\text{C}$  until the next day. Frozen lysates were heated in an  $80^\circ\text{C}$  water bath for 1.5 h, with 15 s of vortexing every 30 min. Methanol concentration of each sample was diluted to 10% by adding 45 mL of water, and cell debris was pelleted by centrifugation at 4,000 g for 10 min. The supernatants were used for the subsequent steps.

All of the following steps were carried out in darkened rooms illuminated with red light to preserve light-sensitive adenosylated corrinoid samples. Solid-phase extraction of adenosylated corrinoids with Sep-Pak C18 cartridges (Waters) was performed as previously described (82). Solvents were evaporated in a vacuum concentrator centrifuge (Savant SPD1010, Thermo Scientific) at  $45^\circ\text{C}$  and the samples were resuspended in 500  $\mu$ L deionized water and passed through 0.45  $\mu$ m pore-size filters (Millex-HV, MilliporeSigma).

Corrinoids were analyzed on an Agilent 1200 series high-performance liquid chromatography (HPLC) system equipped with a diode array detector (Agilent Technologies). Samples were injected into an Agilent Zorbax SB-Aq column (5- $\mu$ m pore size, 4.6 mm  $\times$  150 mm). The following HPLC method was used: solvent A, 0.1% formic acid–deionized water; solvent B, 0.1% formic acid–methanol; flow rate of 1 mL/minute at  $30^\circ\text{C}$ ; 25% to 34% solvent B for 11 min, followed by a linear gradient of 34% to 50% solvent B over 2 min, followed by a linear gradient of 50% to 75% solvent B over 8 min.

**Riboswitch fluorescent reporter assays.** Corrinoid dose-response assays of riboswitch reporter strains were set up as follows. Saturated cultures of the riboswitch reporter strain in LB were diluted 200-fold in LB and dispensed into 96-well microtiter plates (Corning Costar Assay Plate 3904) containing a range of concentrations of various corrinoids. The plates were sealed with gas diffusible membranes (Breathe-Easy, Diversified Biotech) and incubated at  $37^\circ\text{C}$  for 4 to 5 h in a benchtop heated plate shaker (Southwest Science) at 1,200 revolutions per minute (rpm). GFP fluorescence (excitation/emission/bandwidth = 485/525/10 nm) and absorbance at 600 nm ( $A_{600}$ ) were measured on a Tecan Infinite M1000 Pro plate reader. The  $A_{600}$  measurements of uninoculated medium and fluorescence measurements of the parental control strains lacking *gfp* were subtracted from all readings. Data were plotted and analyzed in GraphPad Prism 9.

**3D structural analysis of corrinoids and macromolecular models.** Molecular models of cobalamin in the base-on and base-off/His-on state in complex with various proteins and RNAs were downloaded from the Protein DataBank (PDB) (Table S2) (124). PDB files were analyzed in UCSF Chimera 1.14 (125). Corrinoid molecular models were aligned with each other by the central cobalt atom and coordinating nitrogen atoms of the corrin ring, using the PDB ID 4GMA Cbl model as a reference. Corrinoid models were aligned within the binding sites of riboswitch structures PDB IDs 4GMA, 4FRN, 4GXY, and 6VMY (51, 54, 55).

**Methionine-dependent growth of *B. subtilis* strains.** *B. subtilis* strains were streaked from frozen stocks onto LB agar plates and incubated overnight at  $37^\circ\text{C}$  for 14 to 18 h. Single colonies were used to inoculate 3 mL liquid starter cultures containing Spizizen minimal medium supplemented with 0.02% d-glucose and 0.2% L-Histidine (SMM) (126). Starter cultures of the *metH*-expressing strain were supplemented with 1 nM CNCbl to support growth, whereas the *metE*-expressing strains were cultured in SMM without CNCbl. Starter cultures were incubated overnight shaking (250 rpm,  $37^\circ\text{C}$ ) for 20 h, reaching cell density of about  $\text{OD}_{600} = 1.0$ . Starter cultures were diluted 500-fold by transferring 50  $\mu$ L of starter culture to 25 mL of SMM. Then 75  $\mu$ L of the diluted culture were dispensed into wells of a 96-well microtiter plate containing 75  $\mu$ L of SMM supplemented with 40 nM various corrinoids. Plates were sealed with gas diffusible membranes (Breathe-Easy, Diversified Biotech) and incubated at  $37^\circ\text{C}$  on the “high shaking” setting of a BioTek Synergy2 plate reader. Growth kinetics and *metE* and *metH* expression were measured by  $A_{600}$  and GFP fluorescence every 15 min for 72 h. Data were plotted and analyzed in GraphPad Prism 9.

## SUPPLEMENTAL MATERIAL

Supplemental material is available online only.

**DATA SET S1**, TXT file, 0.03 MB.

**FIG S1**, PDF file, 0.03 MB.

**FIG S2**, PDF file, 0.1 MB.

**FIG S3**, PDF file, 0.2 MB.

**FIG S4**, PDF file, 0.6 MB.

**FIG S5**, PDF file, 0.3 MB.

**FIG S6**, PDF file, 2.1 MB.

**FIG S7**, PDF file, 0.2 MB.

**TABLE S1**, XLSX file, 0.03 MB.

**TABLE S2**, DOCX file, 0.01 MB.

## ACKNOWLEDGMENTS

We thank past and present members of the Taga lab for support. In particular, we thank Sebastian Gude, Zachary Hallberg, and Gordon Pherribo for critical reading of the manuscript; Alexa Nicolas and Amanda Shelton for helpful discussions; Anna Grimaldo and Jong-Duk Park for reagents. We thank Amrita Hazra, Arash Komeili, Michael Marletta, Kathleen Ryan, and Matthew Traxler for helpful discussions. We especially thank Ming Hammond for critical reading of the manuscript and helpful advice. We are grateful to the labs of Benjamin Blackman, John Deuber, Krishna Niyogi, and Matthew Traxler for use of their equipment. This work was supported by NIH grants R01GM114535 and R35GM139633 to M.E.T. We acknowledge that this work was conducted on the ancestral and unceded land of the Ohlone people.

Conceptualization, K.J.K., F.J.W., K.C.M., and M.E.T.; methodology, K.J.K., F.J.W., O.M.S., K.C.M., and M.E.T.; validation: R.R.P.; investigation, K.J.K. and L.V.I.; writing – original draft, K.J.K. and M.E.T.; writing – review & editing, K.J.K., O.M.S., K.C.M., and M.E.T.; funding acquisition, M.E.T.; resources, O.M.S. and K.C.M.; supervision, M.E.T.

We declare no competing interests.

## REFERENCES

- Cech TR, Steitz JA. 2014. The noncoding RNA revolution - trashing old rules to forge new ones. *Cell* 157:77–94. <https://doi.org/10.1016/j.cell.2014.03.008>.
- Roth A, Breaker RR. 2009. The structural and functional diversity of metabolite-binding riboswitches. *Annu Rev Biochem* 78:305–334. <https://doi.org/10.1146/annurev.biochem.78.070507.135656>.
- Winkler WC, Breaker RR. 2005. Regulation of bacterial gene expression by riboswitches. *Annu Rev Microbiol* 59:487–517. <https://doi.org/10.1146/annurev.micro.59.030804.121336>.
- Panchal V, Brenk R. 2021. Riboswitches as drug targets for antibiotics. *Antibiotics* (Basel, Switzerland) 10:45. <https://doi.org/10.3390/antibiotics10010045>.
- Quereda JJ, Cossart P. 2017. Regulating bacterial virulence with RNA. *Annu Rev Microbiol* 71:263–280. <https://doi.org/10.1146/annurev-micro-030117-020335>.
- Wrist A, Sun W, Summers RM. 2020. The theophylline aptamer: 25 years as an important tool in cellular engineering research. *ACS Synth Biol* 9: 682–697. <https://doi.org/10.1021/acssynbio.9b00475>.
- Hallberg ZF, Su Y, Kitto RZ, Hammond MC. 2017. Engineering and *in vivo* applications of riboswitches. *Annu Rev Biochem* 86:515–539. <https://doi.org/10.1146/annurev-biochem-060815-014628>.
- McCown PJ, Corbino KA, Stav S, Sherlock ME, Breaker RR. 2017. Riboswitch diversity and distribution. *RNA* 23:995–1011. <https://doi.org/10.1261/rna.061234.117>.
- Nahvi A, Sudarsan N, Ebert MS, Zou X, Brown KL, Breaker RR. 2002. Genetic control by a metabolite binding mRNA. *Chem Biol* 9:1043. [https://doi.org/10.1016/s1074-5521\(02\)00224-7](https://doi.org/10.1016/s1074-5521(02)00224-7).
- Licht S, Gerfen GJ, Stubbe J. 1996. Thyl radicals in ribonucleotide reductases. *Science* 271:477–481. <https://doi.org/10.1126/science.271.5248.477>.
- Berg IA, Kockelkom D, Buckel W, Fuchs G. 2007. A 3-hydroxypropionate/4-hydroxybutyrate autotrophic carbon dioxide assimilation pathway in Archaea. *Science* 318:1782–1786. <https://doi.org/10.1126/science.1149976>.
- Ljungdahl LG. 1986. The autotrophic pathway of acetate synthesis in acetogenic bacteria. *Annu Rev Microbiol* 40:415–450. <https://doi.org/10.1146/annurev.mi.40.100186.002215>.
- Krasotkina J, Walters T, Maruya KA, Ragsdale SW. 2001. Characterization of the B<sub>12</sub>- and iron-sulfur-containing reductive dehalogenase from *Desulfotobacterium chlororespirans*. *J Biol Chem* 276:40991–40997. <https://doi.org/10.1074/jbc.M106217200>.
- Scarlett FA, Turner JM. 1976. Microbial metabolism of amino alcohols. Ethanolamine catabolism mediated by coenzyme B<sub>12</sub>-dependent ethanolamine ammonia-lyase in *Escherichia coli* and *Klebsiella aerogenes*. *J Gen Microbiol* 95:173–176. <https://doi.org/10.1099/00221287-95-1-173>.
- Stupperich E, Konle R. 1993. Corrinoid-dependent methyl transfer reactions are involved in methanol and 3,4-dimethoxybenzoate metabolism by *Sporomusa ovata*. *Appl Environ Microbiol* 59:3110–3116. <https://doi.org/10.1128/aem.59.9.3110-3116.1993>.
- Jeter RM. 1990. Cobalamin-dependent 1,2-propanediol utilization by *Salmonella typhimurium*. *J Gen Microbiol* 136:887–896. <https://doi.org/10.1099/00221287-136-5-887>.
- Forage RG, Foster MA. 1982. Glycerol fermentation in *Klebsiella pneumoniae*: functions of the coenzyme B<sub>12</sub>-dependent glycerol and diol dehydratases. *J Bacteriol* 149:413–419. <https://doi.org/10.1128/jb.149.2.413-419.1982>.
- Erb TJ, Rétey J, Fuchs G, Alber BE. 2008. Ethylmalonyl-CoA mutase from *Rhodobacter sphaeroides* defines a new subclade of coenzyme B<sub>12</sub>-dependent acyl-CoA mutases. *J Biol Chem* 283:32283–32293. <https://doi.org/10.1074/jbc.M805527200>.
- Korotkova N, Chistoserdova L, Kuksa V, Lidstrom ME. 2002. Glyoxylate regeneration pathway in the methylotroph *Methylobacterium extorquens* AM1. *J Bacteriol* 184:1750–1758. <https://doi.org/10.1128/JB.184.6.1750-1758.2002>.
- Ferguson DJ, Jr., Krzycki JA. 1997. Reconstitution of trimethylamine-dependent coenzyme M methylation with the trimethylamine corrinoid

- protein and the isozymes of methyltransferase II from *Methanosarcina barkeri*. *J Bacteriol* 179:846–852. <https://doi.org/10.1128/jb.179.3.846-852.1997>.
21. Barker HA. 1985. Beta-methylaspartate-glutamate mutase from *Clostridium tetanomorphum*. *Methods Enzymol* 113:121–133. [https://doi.org/10.1016/s0076-6879\(85\)13026-0](https://doi.org/10.1016/s0076-6879(85)13026-0).
  22. Chen HP, Wu SH, Lin YL, Chen CM, Tsay SS. 2001. Cloning, sequencing, heterologous expression, purification, and characterization of adenosylcobalamin-dependent D-ornithine aminomutase from *Clostridium sticklandii*. *J Biol Chem* 276:44744–44750. <https://doi.org/10.1074/jbc.M108365200>.
  23. Chang CH, Frey PA. 2000. Cloning, sequencing, heterologous expression, purification, and characterization of adenosylcobalamin-dependent D-lysine 5, 6-aminomutase from *Clostridium sticklandii*. *J Biol Chem* 275:106–114. <https://doi.org/10.1074/jbc.275.1.106>.
  24. Kim HJ, McCarty RM, Ogasawara Y, Liu Y-n, Mansoorabadi SO, LeVieux J, Liu H-w. 2013. GenK-catalyzed C-6' methylation in the biosynthesis of gentamicin: isolation and characterization of a cobalamin-dependent radical SAM enzyme. *J Am Chem Soc* 135:8093–8096. <https://doi.org/10.1021/ja312641f>.
  25. Knox HL, Chen PY-T, Blaszczyk AJ, Mukherjee A, Grove TL, Schwalm EL, Wang B, Drennan CL, Booker SJ. 2021. Structural basis for non-radical catalysis by TsrM, a radical SAM methylase. *Nat Chem Biol* 17:485–491. <https://doi.org/10.1038/s41589-020-00717-y>.
  26. Choi SC, Bartha R. 1993. Cobalamin-mediated mercury methylation by *Desulfovibrio desulfuricans* L5. *Appl Environ Microbiol* 59:290–295. <https://doi.org/10.1128/aem.59.1.290-295.1993>.
  27. Choi SC, Chase T, Jr., Bartha R. 1994. Enzymatic catalysis of mercury methylation by *Desulfovibrio desulfuricans* L5. *Appl Environ Microbiol* 60:1342–1346. <https://doi.org/10.1128/aem.60.4.1342-1346.1994>.
  28. Parks JM, Johs A, Podar M, Bridou R, Hurt RA, Smith SD, Tomanicek SJ, Qian Y, Brown SD, Brandt CC, Palumbo AV, Smith JC, Wall JD, Elias DA, Liang L. 2013. The genetic basis for bacterial mercury methylation. *Science* 339:1332–1335. <https://doi.org/10.1126/science.1230667>.
  29. Wang P-H, Chen Y-L, Wei ST-S, Wu K, Lee T-H, Wu T-Y, Chiang Y-R. 2020. Retroconversion of estrogens into androgens by bacteria via a cobalamin-mediated methylation. *Proc Natl Acad Sci U S A* 117:1395–1403. <https://doi.org/10.1073/pnas.1914380117>.
  30. Romine MF, Rodionov DA, Maezato Y, Anderson LN, Nandhikonda P, Rodionova IA, Carre A, Li X, Xu C, Clausus TRW, Kim Y-M, Metz TO, Wright AT. 2017. Elucidation of roles for vitamin B<sub>12</sub> in regulation of folate, ubiquinone, and methionine metabolism. *Proc Natl Acad Sci U S A* 114:E1205–E1214. <https://doi.org/10.1073/pnas.1612360114>.
  31. Bridwell-Rabb J, Zhong A, Sun HG, Drennan CL, Liu HW. 2017. A B<sub>12</sub>-dependent radical SAM enzyme involved in oxetanocin A biosynthesis. *Nature* 544:322–326. <https://doi.org/10.1038/nature21689>.
  32. Allen KD, Wang SC. 2014. Initial characterization of Fom3 from *Streptomyces wedmorensis*: the methyltransferase in fosfomycin biosynthesis. *Arch Biochem Biophys* 543:67–73. <https://doi.org/10.1016/j.abb.2013.12.004>.
  33. Pierre S, Guillot A, Benjdia A, Sandström C, Langella P, Berteau O. 2012. Thiostrepton tryptophan methyltransferase expands the chemistry of radical SAM enzymes. *Nat Chem Biol* 8:957–959. <https://doi.org/10.1038/nchembio.1091>.
  34. Marous DR, Lloyd EP, Buller AR, Moshos KA, Grove TL, Blaszczyk AJ, Booker SJ, Townsend CA. 2015. Consecutive radical S-adenosylmethionine methylations form the ethyl side chain in thienamycin biosynthesis. *Proc Natl Acad Sci U S A* 112:10354–10358. <https://doi.org/10.1073/pnas.1508615112>.
  35. Takano H, Mise K, Hagiwara K, Hirata N, Watanabe S, Toriyabe M, Shiratori-Takano H, Ueda K. 2015. Role and function of LitR, an adenosyl B<sub>12</sub>-bound light-sensitive regulator of *Bacillus megaterium* QM B1551, in regulation of carotenoid production. *J Bacteriol* 197:2301–2315. <https://doi.org/10.1128/JB.02528-14>.
  36. Takano H, Kondo M, Usui N, Usui T, Ohzeki H, Yamazaki R, Washioka M, Nakamura A, Hoshino T, Hakamata W, Beppu T, Ueda K. 2011. Involvement of CarA/LitR and CRP/FNR family transcriptional regulators in light-induced carotenoid production in *Thermus thermophilus*. *J Bacteriol* 193:2451–2459. <https://doi.org/10.1128/JB.01125-10>.
  37. Jost M, Fernández-Zapata J, Polanco MC, Ortiz-Guerrero JM, Chen PY-T, Kang G, Padmanabhan S, Elías-Arnanz M, Drennan CL. 2015. Structural basis for gene regulation by a B<sub>12</sub>-dependent photoreceptor. *Nature* 526:536–541. <https://doi.org/10.1038/nature14950>.
  38. Rodionov DA, Vitreschak AG, Mironov AA, Gelfand MS. 2003. Comparative genomics of the vitamin B<sub>12</sub> metabolism and regulation in prokaryotes. *J Biol Chem* 278:41148–41159. <https://doi.org/10.1074/jbc.M305837200>.
  39. Pavlova N, Kaloudas D, Penchovsky R. 2019. Riboswitch distribution, structure, and function in bacteria. *Gene* 708:38–48. <https://doi.org/10.1016/j.gene.2019.05.036>.
  40. Kennedy KJ, Taga ME. 2020. Cobamides. *Curr Biol* 30:R55–R56. <https://doi.org/10.1016/j.cub.2019.11.049>.
  41. Moore SJ, Lawrence AD, Biedendieck R, Deery E, Frank S, Howard MJ, Rigby SEJ, Warren MJ. 2013. Elucidation of the anaerobic pathway for the corrin component of cobalamin (vitamin B<sub>12</sub>). *Proc Natl Acad Sci U S A* 110:14906–14911. <https://doi.org/10.1073/pnas.1308098110>.
  42. Battersby AR. 2000. Tetrapyrroles: the pigments of life. *Nat Prod Rep* 17:507–526. <https://doi.org/10.1039/b002635m>.
  43. Hazra AB, Han AW, Mehta AP, Mok KC, Osadchiv V, Begley TP, Taga ME. 2015. Anaerobic biosynthesis of the lower ligand of vitamin B<sub>12</sub>. *Proc Natl Acad Sci U S A* 112:10792–10797. <https://doi.org/10.1073/pnas.1509132112>.
  44. Chan CH, Escalante-Semerena JC. 2011. ArsAB, a novel enzyme from *Sporomusa ovata* activates phenolic bases for adenosylcobamide biosynthesis. *Mol Microbiol* 81:952–967. <https://doi.org/10.1111/j.1365-2958.2011.07741.x>.
  45. Newmister SA, Chan CH, Escalante-Semerena JC, Rayment I. 2012. Structural insights into the function of the nicotinate mononucleotide:phenol/p-cresol phosphoribosyltransferase (ArsAB) enzyme from *Sporomusa ovata*. *Biochemistry* 51:8571–8582. <https://doi.org/10.1021/bi301142h>.
  46. Yan J, Bi M, Bourdon AK, Farmer AT, Wang P-H, Molenda O, Quaille AT, Jiang N, Yang Y, Yin Y, Şimşir B, Campagna SR, Edwards EA, Löffler FE. 2018. Purinyl-cobamide is a native prosthetic group of reductive dehalogenases. *Nat Chem Biol* 14:8–14. <https://doi.org/10.1038/nchembio.2512>.
  47. Hoffmann B, Oberhuber M, Stupperich E, Bothe H, Buckel W, Konrat R, Kräutler B. 2000. Native corrinoids from *Clostridium cochlearium* are adenylcobamides: spectroscopic analysis and identification of pseudovitamin B<sub>12</sub> and factor A. *J Bacteriol* 182:4773–4782. <https://doi.org/10.1128/JB.182.17.4773-4782.2000>.
  48. Polaski JT, Webster SM, Johnson JE, Jr., Batey RT. 2017. Cobalamin riboswitches exhibit a broad range of ability to discriminate between methylcobalamin and adenosylcobalamin. *J Biol Chem* 292:11650–11658. <https://doi.org/10.1074/jbc.M117.787176>.
  49. Polaski JT, Kletzien OA, Drogalis LK, Batey RT. 2018. A functional genetic screen reveals sequence preferences within a key tertiary interaction in cobalamin riboswitches required for ligand selectivity. *Nucleic Acids Res* 46:9094–9105. <https://doi.org/10.1093/nar/gky539>.
  50. Gallo S, Oberhuber M, Sigel RK, Kräutler B. 2008. The corrin moiety of coenzyme B<sub>12</sub> is the determinant for switching the *btuB* riboswitch of *E. coli*. *Chembiochem* 9:1408–1414. <https://doi.org/10.1002/cbic.200800099>.
  51. Chan CW, Mondragón A. 2020. Crystal structure of an atypical cobalamin riboswitch reveals RNA structural adaptability as basis for promiscuous ligand binding. *Nucleic Acids Res* 48:7569–7583. <https://doi.org/10.1093/nar/gkaa507>.
  52. Stupperich E, Eisinger HJ, Kräutler B. 1988. Diversity of corrinoids in acetogenic bacteria. P-cresolcobamide from *Sporomusa ovata*, 5-methoxy-6-methylbenzimidazolylcobamide from *Clostridium formicoaceticum* and vitamin B<sub>12</sub> from *Acetobacterium woodii*. *Eur J Biochem* 172:459–464. <https://doi.org/10.1111/j.1432-1033.1988.tb13910.x>.
  53. Crofts TS, Seth EC, Hazra AB, Taga ME. 2013. Cobamide structure depends on both lower ligand availability and CobT substrate specificity. *Chem Biol* 20:1265–1274. <https://doi.org/10.1016/j.chembiol.2013.08.006>.
  54. Johnson JE, Jr., Reyes FE, Polaski JT, Batey RT. 2012. B<sub>12</sub> cofactors directly stabilize an mRNA regulatory switch. *Nature* 492:133–137. <https://doi.org/10.1038/nature11607>.
  55. Peselis A, Serganov A. 2012. Structural insights into ligand binding and gene expression control by an adenosylcobalamin riboswitch. *Nat Struct Mol Biol* 19:1182–1184. <https://doi.org/10.1038/nsmb.2405>.
  56. Barker HA, Smyth RD, Weissbach H, Toohey JI, Ladd JN, Volcani BE. 1960. Isolation and properties of crystalline cobamide coenzymes containing benzimidazole or 5,6-dimethylbenzimidazole. *J Biol Chem* 235:480–488. [https://doi.org/10.1016/S0021-9258\(18\)69550-X](https://doi.org/10.1016/S0021-9258(18)69550-X).
  57. Ladd JN, Hogenkamp HP, Barker HA. 1961. Structure of cobamide coenzymes: influence of pH on absorption spectra and ionophoretic mobilities. *J Biol Chem* 236:2114–2118. [https://doi.org/10.1016/S0021-9258\(18\)64138-9](https://doi.org/10.1016/S0021-9258(18)64138-9).
  58. Brown KL, Hakimi JM. 1986. Heteronuclear NMR studies of cobalamins. 4. alpha-Ribazole-3'-phosphate and the nucleotide loop of base-on cobalamins. *J Am Chem Soc* 108:496–503. <https://doi.org/10.1021/ja00263a023>.
  59. Fieber W, Hoffmann B, Schmidt W, Stupperich E, Konrat R, Kräutler B. 2002. Pseudocoenzyme B<sub>12</sub> and adenosyl-Factor A: electrochemical synthesis and spectroscopic analysis of two natural B<sub>12</sub> coenzymes with



- predominantly 'base-off' constitution. *Hca* 85:927–944. [https://doi.org/10.1002/1522-2675\(200203\)85:3%3C927::AID-HLCA927%3E3.0.CO;2-A](https://doi.org/10.1002/1522-2675(200203)85:3%3C927::AID-HLCA927%3E3.0.CO;2-A).
60. Marques HM, Zou X, Brown KL. 2000. The solution structure of adenosylcobalamin and adenosylcobinamide determined by nOe-restrained molecular dynamics simulations. *J Molecular Structure* 520:75–95. [https://doi.org/10.1016/S0022-2860\(99\)00309-9](https://doi.org/10.1016/S0022-2860(99)00309-9).
  61. Sussman D, Wilson C. 2000. A water channel in the core of the vitamin B<sub>12</sub> RNA aptamer. *Structure* 8:719–727. [https://doi.org/10.1016/S0969-2126\(00\)00159-3](https://doi.org/10.1016/S0969-2126(00)00159-3).
  62. Mancia F, Keep NH, Nakagawa A, Leadlay PF, McSweeney S, Rasmussen B, Bösecke P, Diat O, Evans PR. 1996. How coenzyme B<sub>12</sub> radicals are generated: the crystal structure of methylmalonyl-coenzyme A mutase at 2 Å resolution. *Structure* 4:339–350. [https://doi.org/10.1016/S0969-2126\(96\)00037-8](https://doi.org/10.1016/S0969-2126(96)00037-8).
  63. Froese DS, Kochan G, Muniz JRC, Wu X, Gileadi C, Ugochukwu E, Krysztofinska E, Gravel RA, Oppermann U, Yue WW. 2010. Structures of the human GTPase MMAA and vitamin B<sub>12</sub>-dependent methylmalonyl-CoA mutase and insight into their complex formation. *J Biol Chem* 285:38204–38213. <https://doi.org/10.1074/jbc.M110.177717>.
  64. Drennan CL, Huang S, Drummond JT, Matthews RG, Ludwig ML. 1994. How a protein binds B<sub>12</sub>: a 3.0 Å X-ray structure of B<sub>12</sub>-binding domains of methionine synthase. *Science* 266:1669–1674. <https://doi.org/10.1126/science.7992050>.
  65. Dowling DP, Miles ZD, Köhrer C, Maiocco SJ, Elliott SJ, Bandarian V, Drennan CL. 2016. Molecular basis of cobalamin-dependent RNA modification. *Nucleic Acids Res* 44:9965–9976. <https://doi.org/10.1093/nar/gkw806>.
  66. Payne KAP, Fisher K, Sjuts H, Dunstan MS, Bellina B, Johannissen L, Barran P, Hay S, Rigby SEJ, Leys D. 2015. Epoxyqueuosine reductase structure suggests a mechanism for cobalamin-dependent tRNA modification. *J Biol Chem* 290:27572–27581. <https://doi.org/10.1074/jbc.M115.685693>.
  67. Payne KA, Quezada CP, Fisher K, Dunstan MS, Collins FA, Sjuts H, Levy C, Hay S, Rigby SE, Leys D. 2015. Reductive dehalogenase structure suggests a mechanism for B<sub>12</sub>-dependent dehalogenation. *Nature* 517:513–516. <https://doi.org/10.1038/nature13901>.
  68. Jost M, Born DA, Cracan V, Banerjee R, Drennan CL. 2015. Structural basis for substrate specificity in adenosylcobalamin-dependent isobutyryl-CoA mutase and related Acyl-CoA mutases. *J Biol Chem* 290:26882–26898. <https://doi.org/10.1074/jbc.M115.676890>.
  69. Gruber K, Reitzer R, Kratky C. 2001. Radical shuttling in a protein: ribose pseudorotation controls alkyl-radical transfer in the coenzyme B<sub>12</sub>-dependent enzyme glutamate mutase. *Angew Chem Int Ed* 40:3377–3380. [https://doi.org/10.1002/1521-3773\(20010917\)40:18%3C3377::AID-ANIE3377%3E3.0.CO;2-8](https://doi.org/10.1002/1521-3773(20010917)40:18%3C3377::AID-ANIE3377%3E3.0.CO;2-8).
  70. Berkovitch F, Behshad E, Tang K-H, Enns EA, Frey PA, Drennan CL. 2004. A locking mechanism preventing radical damage in the absence of substrate, as revealed by the x-ray structure of lysine 5,6-aminomutase. *Proc Natl Acad Sci U S A* 101:15870–15875. <https://doi.org/10.1073/pnas.0407074101>.
  71. Lussier A, Bastet L, Chauvier A, Lafontaine DA. 2015. A kissing loop is important for *btuB* riboswitch ligand sensing and regulatory control. *J Biol Chem* 290:26739–26751. <https://doi.org/10.1074/jbc.M115.684134>.
  72. Polaski JT, Holmstrom ED, Nesbitt DJ, Batey RT. 2016. Mechanistic insights into cofactor-dependent coupling of RNA folding and mRNA transcription/translation by a cobalamin riboswitch. *Cell Rep* 15:1100–1110. <https://doi.org/10.1016/j.celrep.2016.03.087>.
  73. Mukherjee S, Das Mandal V, Banerjee N, Drory-Retwitzer M, Barash D, Sengupta S. 2019. RibodB: a comprehensive database for prokaryotic riboswitches. *Bioinformatics* 35:3541–3543. <https://doi.org/10.1093/bioinformatics/btz093>.
  74. Sudarsan N, Hammond MC, Block KF, Welz R, Barrick JE, Roth A, Breaker RR. 2006. Tandem riboswitch architectures exhibit complex gene control functions. *Science* 314:300–304. <https://doi.org/10.1126/science.1130716>.
  75. Moore SJ, Mayer MJ, Biedendieck R, Deery E, Warren MJ. 2014. Towards a cell factory for vitamin B<sub>12</sub> production in *Bacillus megaterium*: bypassing of the cobalamin riboswitch control elements. *N Biotechnol* 31:553–561. <https://doi.org/10.1016/j.nbt.2014.03.003>.
  76. Collins HF, Biedendieck R, Leech HK, Gray M, Escalante-Semerena JC, McLean KJ, Munro AW, Rigby SEJ, Warren MJ, Lawrence AD. 2013. *Bacillus megaterium* has both a functional BluB protein required for DMB synthesis and a related flavoprotein that forms a stable radical species. *PLoS One* 8:e55708. <https://doi.org/10.1371/journal.pone.0055708>.
  77. Biedendieck R, Malten M, Barg H, Bunk B, Martens J-H, Deery E, Leech H, Warren MJ, Jahn D. 2010. Metabolic engineering of cobalamin (vitamin B<sub>12</sub>) production in *Bacillus megaterium*. *Microb Biotechnol* 3:24–37. <https://doi.org/10.1111/j.1751-7915.2009.00125.x>.
  78. Ma AT, Tyrell B, Beld J. 2020. Specificity of cobamide remodeling, uptake and utilization in *Vibrio cholerae*. *Mol Microbiol* 113:89–102. <https://doi.org/10.1111/mmi.14402>.
  79. Degnan PH, Barry NA, Mok KC, Taga ME, Goodman AL. 2014. Human gut microbes use multiple transporters to distinguish vitamin B<sub>12</sub> analogs and compete in the gut. *Cell Host Microbe* 15:47–57. <https://doi.org/10.1016/j.chom.2013.12.007>.
  80. Tanioka Y, Miyamoto E, Yabuta Y, Ohnishi K, Fujita T, Yamaji R, Misono H, Shigeoka S, Nakano Y, Inui H, Watanabe F. 2010. Methyladeninylcobamide functions as the cofactor of methionine synthase in a Cyanobacterium, *Spirulina platensis* NIES-39. *FEBS Lett* 584:3223–3226. <https://doi.org/10.1016/j.febslet.2010.06.013>.
  81. Helliwell KE, Lawrence AD, Holzer A, Kudahl UJ, Sasso S, Kräutler B, Scanlan DJ, Warren MJ, Smith AG. 2016. Cyanobacteria and eukaryotic algae use different chemical variants of vitamin B<sub>12</sub>. *Curr Biol* 26:999–1008. <https://doi.org/10.1016/j.cub.2016.02.041>.
  82. Sokolovskaya OM, Mok KC, Park JD, Tran JLA, Quanstrom KA, Taga ME. 2019. Cofactor selectivity in methylmalonyl coenzyme A mutase, a model cobamide-dependent enzyme. *mBio* 10:e01303-19. <https://doi.org/10.1128/mBio.01303-19>.
  83. Nahvi A, Barrick JE, Breaker RR. 2004. Coenzyme B<sub>12</sub> riboswitches are widespread genetic control elements in prokaryotes. *Nucleic Acids Res* 32:143–150. <https://doi.org/10.1093/nar/gkh167>.
  84. Gallo S, Mundwiler S, Alberto R, Sigel RK. 2011. The change of corrinamides to carboxylates leads to altered structures of the B<sub>12</sub>-responding *btuB* riboswitch. *Chem Commun (Camb)* 47:403–405. <https://doi.org/10.1039/c0cc02447c>.
  85. Choudhary PK, Duret A, Rohrbach-Brandt E, Holliger C, Sigel RKO, Maillard J. 2013. Diversity of cobalamin riboswitches in the corrinoid-producing organohalide respirer *Desulfitobacterium hafniense*. *J Bacteriol* 195:5186–5195. <https://doi.org/10.1128/JB.00730-13>.
  86. Di Girolamo PM, Kadner RJ, Bradbeer C. 1971. Isolation of vitamin B<sub>12</sub> transport mutants of *Escherichia coli*. *J Bacteriol* 106:751–757. <https://doi.org/10.1128/jb.106.3.751-757.1971>.
  87. Kashket S, Kaufman JT, Beck WS. 1962. The metabolic functions of vitamin B<sub>12</sub>. III. Vitamin B<sub>12</sub> binding in *Lactobacillus leichmannii* and other lactobacilli. *Biochim Biophys Acta* 64:447–457. [https://doi.org/10.1016/0006-3002\(62\)90302-5](https://doi.org/10.1016/0006-3002(62)90302-5).
  88. Giannella RA, Broitman SA, Zamcheck N. 1971. Vitamin B<sub>12</sub> uptake by intestinal microorganisms: mechanism and relevance to syndromes of intestinal bacterial overgrowth. *J Clin Invest* 50:1100–1107. <https://doi.org/10.1172/JCI106581>.
  89. Price IR, Grigg JC, Ke A. 2014. Common themes and differences in SAM recognition among SAM riboswitches. *Biochim Biophys Acta* 1839:931–938. <https://doi.org/10.1016/j.bbtagrm.2014.05.013>.
  90. Huang L, Liao TW, Wang J, Ha T, Lilley DMJ. 2020. Crystal structure and ligand-induced folding of the SAM/SAH riboswitch. *Nucleic Acids Res* 48:7545–7556. <https://doi.org/10.1093/nar/gkaa493>.
  91. Weickhmann AK, Keller H, Wurm JP, Streibitzer E, Juen MA, Kremser J, Weinberg Z, Kreutz C, Duchardt-Ferner E, Wöhnert J. 2019. The structure of the SAM/SAH-binding riboswitch. *Nucleic Acids Res* 47:2654–2665. <https://doi.org/10.1093/nar/gky1283>.
  92. Ma B, Bai G, Nussinov R, Ding J, Wang YX. 2021. Conformational ensemble of *TteAdoCbl* riboswitch provides stable structural elements for conformation selection and population shift in cobalamin recognition. *J Phys Chem B* 125:2589–2596. <https://doi.org/10.1021/acs.jpcc.1c00038>.
  93. Trausch JJ, Batey RT. 2014. A disconnect between high-affinity binding and efficient regulation by antifolates and purines in the tetrahydrofolate riboswitch. *Chem Biol* 21:205–216. <https://doi.org/10.1016/j.chembiol.2013.11.012>.
  94. Shelton AN, Lyu X, Taga ME. 2020. Flexible cobamide metabolism in *Clostridioides (Clostridium) difficile* 630 Δerm. *J Bacteriol* 202 <https://doi.org/10.1128/JB.00584-19>.
  95. Mok KC, Taga ME. 2013. Growth inhibition of *Sporomusa ovata* by incorporation of benzimidazole bases into cobamides. *J Bacteriol* 195:1902–1911. <https://doi.org/10.1128/JB.01282-12>.
  96. Shelton AN, Seth EC, Mok KC, Han AW, Jackson SN, Haft DR, Taga ME. 2019. Uneven distribution of cobamide biosynthesis and dependence in bacteria predicted by comparative genomics. *ISME J* 13:789–804. <https://doi.org/10.1038/s41396-018-0304-9>.
  97. Fedosov SN, Fedosova NU, Kräutler B, Nexø E, Petersen TE. 2007. Mechanisms of discrimination between cobalamins and their natural analogues

- during their binding to the specific B<sub>12</sub>-transporting proteins. *Biochemistry* 46:6446–6458. <https://doi.org/10.1021/bi062063l>.
98. Chan CH, Newmister SA, Talyor K, Claas KR, Rayment I, Escalante-Semerena JC. 2014. Dissecting cobamide diversity through structural and functional analyses of the base-activating CobT enzyme of *Salmonella enterica*. *Biochim Biophys Acta* 1840:464–475. <https://doi.org/10.1016/j.bbagen.2013.09.038>.
  99. Hazra AB, Tran JL, Crofts TS, Taga ME. 2013. Analysis of substrate specificity in CobT homologs reveals widespread preference for DMB, the lower axial ligand of vitamin B<sub>12</sub>. *Chem Biol* 20:1275–1285. <https://doi.org/10.1016/j.chembiol.2013.08.007>.
  100. Cheong CG, Escalante-Semerena JC, Rayment I. 2001. Structural investigation of the biosynthesis of alternative lower ligands for cobamides by nicotinate mononucleotide:5,6-dimethylbenzimidazole phosphoribosyltransferase from *Salmonella enterica*. *J Biol Chem* 276:37612–37620. <https://doi.org/10.1074/jbc.M105390200>.
  101. Cheong CG, Escalante-Semerena JC, Rayment I. 1999. The three-dimensional structures of nicotinate mononucleotide:5,6-dimethylbenzimidazole phosphoribosyltransferase (CobT) from *Salmonella typhimurium* complexed with 5,6-dimethylbenzimidazole and its reaction products determined to 1.9 Å resolution. *Biochemistry* 38:16125–16135. <https://doi.org/10.1021/bi991752c>.
  102. Trzebiatowski JR, Escalante-Semerena JC. 1997. Purification and characterization of CobT, the nicotinate-monomonucleotide:5,6-dimethylbenzimidazole phosphoribosyltransferase enzyme from *Salmonella typhimurium* LT2. *J Biol Chem* 272:17662–17667. <https://doi.org/10.1074/jbc.272.28.17662>.
  103. Trzebiatowski JR, O'Toole GA, Escalante-Semerena JC. 1994. The *cobT* gene of *Salmonella typhimurium* encodes the NaMN: 5,6-dimethylbenzimidazole phosphoribosyltransferase responsible for the synthesis of N1-(5-phospho- $\alpha$ -D-ribose)-5,6-dimethylbenzimidazole, an intermediate in the synthesis of the nucleotide loop of cobalamin. *J Bacteriol* 176:3568–3575. <https://doi.org/10.1128/jb.176.12.3568-3575.1994>.
  104. Sokolovskaya OM, Shelton AN, Taga ME. 2020. Sharing vitamins: cobamides unveil microbial interactions. *Science* 369 <https://doi.org/10.1126/science.aba0165>.
  105. Villa JK, Su Y, Contreras LM, Hammond MC. 2018. Synthetic biology of small RNAs and riboswitches. *Microbiol Spectr* 6 <https://doi.org/10.1128/microbiolspec.RWR-0007-2017>.
  106. Galizi R, Jaramillo A. 2019. Engineering CRISPR guide RNA riboswitches for *in vivo* applications. *Curr Opin Biotechnol* 55:103–113. <https://doi.org/10.1016/j.copbio.2018.08.007>.
  107. Mansjö M, Johansson J. 2011. The riboflavin analog roseoflavin targets an FMN-riboswitch and blocks *Listeria monocytogenes* growth, but also stimulates virulence gene-expression and infection. *RNA Biol* 8:674–680. <https://doi.org/10.4161/rna.8.4.15586>.
  108. Kräutler B. 2020. Antivitamins B<sub>12</sub> - some inaugural milestones. *Chemistry* 26:15438–15445. <https://doi.org/10.1002/chem.202003788>.
  109. Zelder F, Sonnay M, Prieto L. 2015. Antivitamins for medicinal applications. *ChemBiochem* 16:1264–1278. <https://doi.org/10.1002/cbic.201500072>.
  110. Mukherjee S, Sengupta S. 2016. Riboswitch Scanner: an efficient pHMM-based web-server to detect riboswitches in genomic sequences. *Bioinformatics* 32:776–778. <https://doi.org/10.1093/bioinformatics/btv640>.
  111. Singh P, Bandyopadhyay P, Bhattacharya S, Krishnamachari A, Sengupta S. 2009. Riboswitch detection using profile hidden Markov models. *BMC Bioinformatics* 10:325. <https://doi.org/10.1186/1471-2105-10-325>.
  112. Mathews DH, Disney MD, Childs JL, Schroeder SJ, Zuker M, Turner DH. 2004. Incorporating chemical modification constraints into a dynamic programming algorithm for prediction of RNA secondary structure. *Proc Natl Acad Sci U S A* 101:7287–7292. <https://doi.org/10.1073/pnas.0401799101>.
  113. Reuter JS, Mathews DH. 2010. RNAstructure: software for RNA secondary structure prediction and analysis. *BMC Bioinformatics* 11:129. <https://doi.org/10.1186/1471-2105-11-129>.
  114. Wilson KS, von Hippel PH. 1995. Transcription termination at intrinsic terminators: the role of the RNA hairpin. *Proc Natl Acad Sci U S A* 92:8793–8797. <https://doi.org/10.1073/pnas.92.19.8793>.
  115. Gusarov I, Nudler E. 1999. The mechanism of intrinsic transcription termination. *Mol Cell* 3:495–504. [https://doi.org/10.1016/s1097-2765\(00\)80477-3](https://doi.org/10.1016/s1097-2765(00)80477-3).
  116. Waterhouse AM, Procter JB, Martin DM, Clamp M, Barton GJ. 2009. Jalview Version 2—a multiple sequence alignment editor and analysis workbench. *Bioinformatics* 25:1189–1191. <https://doi.org/10.1093/bioinformatics/btp033>.
  117. Sokolovskaya OM, Plessl T, Bailey H, Mackinnon S, Baumgartner MR, Yue WW, Froese DS, Taga ME. 2020. Naturally occurring cobalamin (B<sub>12</sub>) analogs can function as cofactors for human methylmalonyl-CoA mutase. *Biochimica* 183:35–143.
  118. Yi S, Seth EC, Men Y-J, Stabler SP, Allen RH, Alvarez-Cohen L, Taga ME. 2012. Versatility in corrinoid salvaging and remodeling pathways supports corrinoid-dependent metabolism in *Dehalococcoides mccartyi*. *Appl Environ Microbiol* 78:7745–7752. <https://doi.org/10.1128/AEM.02150-12>.
  119. Mok KC, Sokolovskaya OM, Nicolas AM, Hallberg ZF, Deutschbauer A, Carlson HK, Taga ME. 2020. Identification of a novel cobamide remodeling enzyme in the beneficial human gut bacterium *Akkermansia muciniphila*. *mBio* 11:e02507-20. <https://doi.org/10.1128/mBio.02507-20>.
  120. Gibson DG, Young L, Chuang R-Y, Venter JC, Hutchison CA, Smith HO. 2009. Enzymatic assembly of DNA molecules up to several hundred kilobases. *Nat Methods* 6:343–345. <https://doi.org/10.1038/nmeth.1318>.
  121. Guiziou S, Sauveplane V, Chang H-J, Clercé C, Declercq N, Jules M, Bonnet J. 2016. A part toolbox to tune genetic expression in *Bacillus subtilis*. *Nucleic Acids Res* 44:7495–7508. <https://doi.org/10.1093/nar/gkw624>.
  122. Zhang XZ, Zhang Y. 2011. Simple, fast and high-efficiency transformation system for directed evolution of cellulase in *Bacillus subtilis*. *Microb Biotechnol* 4:98–105. <https://doi.org/10.1111/j.1751-7915.2010.00230.x>.
  123. Koo B-M, Kritikos G, Farelli JD, Todor H, Tong K, Kimsey H, Wapinski I, Galardini M, Cabal A, Peters JM, Hachmann A-B, Rudner DZ, Allen KN, Typas A, Gross CA. 2017. Construction and analysis of two genome-scale deletion libraries for *Bacillus subtilis*. *Cell Syst* 4:291–305. <https://doi.org/10.1016/j.cels.2016.12.013>.
  124. Berman HM, Westbrook J, Feng Z, Gilliland G, Bhat TN, Weissig H, Shindyalov IN, Bourne PE. 2000. The protein data bank. *Nucleic Acids Res* 28:235–242. <https://doi.org/10.1093/nar/28.1.235>.
  125. Pettersen EF, Goddard TD, Huang CC, Couch GS, Greenblatt DM, Meng EC, Ferrin TE. 2004. UCSF chimera—a visualization system for exploratory research and analysis. *J Comput Chem* 25:1605–1612. <https://doi.org/10.1002/jcc.20084>.
  126. Anagnostopoulos C, Spizizen J. 1961. Requirements for transformation in *Bacillus subtilis*. *J Bacteriol* 81:741–746. <https://doi.org/10.1128/jb.81.5.741-746.1961>.